UNIVERSITY OF TURKU

Ionospheric Regional modeling Algorithm based on GNSS Precise Point Positioning

Smart Systems

Master's Degree Programme in Information and Communication Technology

Department of Computing, Faculty of Technology

Master of Science in Technology Thesis

Author:

Yan Chen

Supervisors:

Ph.D Tuan Nguyen

Professor Haiyang Fu (Fudan University)

Sep. 2021

The originality of this thesis has been checked in accordance with the University of Turku quality assurance system using the Turnitin Originality Check service.

Master of Science in Technology Thesis
Department of Computing, Faculty of Technology
University of Turku

Subject: Smart Systems
Programme: Master's Degree Programme in Information and Communication Technology
Author: Yan Chen
Title: Ionospheric Regional modeling Algorithm based on GNSS Precise Point Positioning
Number of pages: 71 pages, 0 appendix pages
Date: 09 2021

Abstract

Precise point positioning (PPP) is an absolute spatial positioning technology different from carrier phase relative positioning. With the continuous development of Global navigation satellite system (GNSS), multi-constellation GNSS further provides PPP with more abundant observation information and useful spatial geometric observations, which improves positioning performance and robustness. In recent years, the un-difference and un-combined precise point positioning (UPPP) has been continuously developing. Firstly, we introduce the basic theory of GNSS positioning and compare the position performance between UPPP and ionospheric-free PPP (IF PPP). The positioning performance of the four mainstream GNSS systems, GPS, GLONASS, Galileo, and Beidou, the PPP floating-point solutions of the four satellite systems all converge within 60 minutes and their error are less than 10cm. Secondly, a two-dimensional (2-d) model is proposed to fit the vertical total electronic content (VTEC) in the ionosphere with the ionospheric delays extracted by UPPP. With the model constraining the ionospheric delay in UPPP, the convergence is 2 minutes shorter than using the global ionospheric map (GIM) from IGS. Thirdly, to solve the limitation of the traditional methods in 2d representation, a method is proposed represent the ionosphere in 3D, called Compressed Sensing Tomography (CST). Comparing the simulated single-difference slant total electron content (STEC) and the input single-difference STEC between satellites, the root mean square (RMS) of the reference station's error is less than 1 TEC unit.

Keywords: Precise point positioning (PPP), Ionospheric delay, mathematical model of VTEC, Compressed Sensing Tomography (CST).

Table of contents

List of Abbreviations

Abbreviations	Definition
2D	Two-Dimensional
3D	Three-Dimensional
ART	Algebraic Reconstruction Technology
BDS	BeiDou Navigation Satellite System
CAS	Chinese Academy of Sciences
CODE	Center for Orbit Determination in Europe
CORS	Continuously Operating Reference Stations
CST	Compressed Sensing Tomography
DCB	Differential Code Bias
DGNSS	Differential Global Navigation Satellite System
DOP	Dilution of Precision
dSTEC	Differential Slant Total Electronic Content
ESA	European Space Agency
GAL	Galileo Satellite Navigation System
GDOP	Geometric Dilution of Precision
GF	Geometry-free Combination
GIM	Global Ionosphere Map
GLONASS	Global Orbiting Navigation Satellite System
GNSS	Global Navigation Satellite System
GPS	Global Positioning System
HDOP	Horizontal Dilution of Precision
IF PPP	Ionosphere-free Precise Point Positioning
IGS	International GNSS Service Organization
IRI	International Reference Ionospheric Model
IRNSS	Indian Regional Navigation Satellite System
ISR	Incoherent Scattering Radar
JPL	Jet Propulsion Laboratory
LSQ	Least Square Method

KF	Kalman Filter
M-SLM	Modified Single Layer Mapping
MW	Melbourne-Wubeena Combination
NEU	North-East-Up Coordinate
PCA	Principal Components Analysis
PCO	Phase Center Offset
PCV	Phase Center Variation
PPP	Precise Point Positioning
PPP-AR	precise Point Positioning based on Ambiguity Resolution
PPP-RTK	Precise Point Positioning-Real-Time Kinematic
QZSS	Quasi-Zenith Satellite System
RAIM	Receiver Autonomous Integrity Monitoring
RTK	Real-time Kinematic Positioning
SBAS	Satellite-Based Augmentation System
SLM	Single Layer Mapping
SNR	Signal Noise Ratio
SPP	Single Point Positioning
STEC	Slant Total Electronic Content
SVD	Singular Value Decomposition
TEC	Total Electronic Content
TECU	Total Electronic Content Unit
TGD	Timing Group Delay
TLS	Total Least Squares
UPC	Technical University of Catalonia
UPPP	Un-difference and Un-combined Precise Point Positioning
VDOP	Vertical Dilution of Precision
VTEC	Vertical Total Electronic Content
WL	Wide Lane

1 Introduction

1.1 Overview

After the satellite navigation system service first appeared in the 1970s, it has undergone more than 40 years of development and improvement. Recently, with the Global Navigation Satellite System (GNSS) developing, the constellation structure and positioning performance have improved significantly. It consists of four main systems such as the GPS by USA, GLONASS by Russia, Galileo by Europe and BDS by China. In addition, there are some other regional systems like QZSS (Japan) and IRNSS (India). Besides, there are various satellite-based augmentation systems (SBAS) [1]. Concurrently, the data processing methods of navigation satellites continue to develop, including Doppler positioning, pseudo-range single point positioning (SPP), pseudo-range differential positioning (DGNSS), real-time kinematic positioning (RTK), precise point positioning (PPP), network RTK, un-difference network PPP –RTK [1]. Each positioning algorithm has its advantages and limitations. Among them, Doppler positioning and SPP have low positioning accuracy. DGNSS has a small use range due to the mismatch between use cost and positioning performance with the influence of the low signal-to-noise ratio (SNR). RTK and network RTK are technologies that are real-time and high-precision positioning. However, in the technology with RTK as the core, the cooperation of base stations is required, which will increase application costs for most users.

To gain a high precise position and lower cost, PPP has become an inevitable choice. PPP is an absolute positioning method. It uses the precise satellite orbits and clock error correction products provided by the International GNSS Service Organization (IGS) [2][3], comprehensively considering the accurate revision of various error models, utilizing pseudo-range and carrier phase observations of one receiver. Although PPP has developed for two decades, and applications and research related to PPP still have been appeared. PPP still faces a series of crucial technological breakthroughs in practical applications. First, due to the technical characteristics of PPP (un-difference observation equation), it cannot use the inter-station difference to decrease the adverse influences of related errors on the positioning results, mostly due to the influences of unchecked initial phase deviation. It will result in un-difference ambiguity parameters losing the integer characteristics, obtaining PPP floating-point solutions. Secondly, due to factors such as pseudo-range noise, atmospheric delay error, multipath, and other error sources, the initialization time of PPP is much longer than other

methods. To gain a centimeter-level or even millimeter-level positioning results, it usually costs 30 minutes or more for the first initialization time. The complicated environment may cause the signal unlocking. And the re-initialization after the satellites unlocking also needs a long time. The time is almost equal to the first initialization time.

What is more serious is that the receiver clock jumps and ionospheric scatter will also affect the accuracy of PPP data processing. It may cause some unnecessary re-initialization processes and significantly reduce its accuracy and efficiency. With multiple GNSS systems' development, the combined positioning of multiple GNSS systems has much more satellites and suitable spatial geometry, which can obtain more useful observation data. As a result, it effectively improves positioning accuracy and shortens the convergence time. Meanwhile, the use of an accurate ionospheric prior model can also significantly enhance the convergence speed. In this thesis, we use open-source observation data such as international GNSS reference sites or American CORS sites to position and extract the ionospheric delay through UPPP. Then, the ionospheric delay estimated are fitted by a certain model. PPP users using a priori ionospheric delay data as a constraint can significantly decrease the positioning initialization time and effectively improve the positioning performance.

At present, more and more reference station networks are being established and improved domestic and foreign. Regional reference stations can provide more GNSS observations, which promote scholars or institutions to do much work to obtain high-precision ionospheric data by processing the data. The popular ionospheric models is separated into two types. One is using lots of prior observation data to analyse and fit a priori three-dimensional (3D) electron density model, such as the International Reference Ionospheric Model (IRI) [4], the NeQuick model [5], etc. These models have large fitting errors. The other is the real-time ionospheric delay extracted from the observations of the regional reference station network. Then, use these data to fit the ionosphere with the mathematical model [6]. This method brings less error than the prior model. Due to the large real-time observations, the correction satisfies the request of the PPP.

In summary, PPP can achieve high-precision absolute positioning, and regional observation stations can obtain better ionospheric delay. Extracting ionospheric delay through the regional stations' observations and modeling the ionospheric delay also has essential significance for high-precision positioning.

1.2 Precise point positioning

The method, Precise point position (PPP) was first published in 1997 by researchers (Zumberge. et al) at the Jet Propulsion Laboratory [2]. They proposed that a single receiver can use precise ephemeris and precise clock offsets rather than the traditional broadcast ephemeris to process single-point positioning. And it can easily reach centimeter-level positioning. Later, NRCan of the Canadian Ministry of Natural Resources (Kouba et al.) combined pseudo-range and carrier phase observations to eliminate the ionospheric first-order effect, gaining centimeters results [7]. However, the noise of the traditional ionosphere-free model is nearly three times larger than the original observations. In 2002, Gao et al. of Calgary University proposed the method that using the ionosphere-free model and Half-sum combination of code and phase, called Uofc model [8]. The model is reduced by half compared with the original observations. In 2006, Keshin et al. put forward UPPP, which puts a tropospheric and ionospheric delay as a solution [9]. In 2008 and 2009, several teams (Paul Collins et al., Ge et al., Laurichesse et al.) proposed the UPPP with the ambiguity resolution (PPP-AR), which reduces the convergence time apparently [10][11][12]. In 2010, Zhang focused on UPPP algorithm based on GPS raw dual-frequency pseudo-range, carrier phase data and tried to extract high-precision ionospheric delay values from the UPPP [13]. Geng et al. used triple-frequency to perform PPP-AR, improving the success rate of gaining ambiguity resolution [14]. Li et al. used GPS, GLONASS, Galileo, and BeiDou to position, comparing their performance, respectively, in 2016 [15]. In 2018, Zhang discussed the theoretical and practical aspects of PPP-RTK [16].

In conclusion, The UPPP can effectively use the observation information and extract the required parameter information. With the improvement of GNSS and PPP algorithm, the positioning accuracy and convergence are better than existing methods, which has become a popular aspect of current research.

1.3 Ionosphere extraction and modeling

Ionospheric delay is the most influential error source in GNSS positioning, and the maximum impact on the positioning can reach 100 meters. Scholars are committed to studying how to build a high-precision ionospheric model to decrease the influence of the ionosphere.

The first step of the modeling is to extract the ionospheric delay. In 1985, Bishop and Klobuchar utilized the relationship between ionospheric delay and frequency, which is named

the geometry-free method [17]. The method contains a few other noises and is unreliable. In 1999, Schaer used carrier phase smoothed code to decrease the effect of the noise [18]. Zhang suggested that using carrier phase smoothed code method contain more massive error at night, so he improved the UPPP method, using UPPP to extract the ionospheric delay. It decreases the effects of the multipath and observable noise, making the extracted results more accurate [19]. However, the UPPP method cannot eliminate the impacts, so there is still a long way to find a better approach.

The existing ionospheric models contain two aspects including empirical models that reflect the changes in the ionosphere based on a large number of observations, such as the IRI model [4], NeQuick model [5], Klobuchar model [1]. The other one is a mathematical model fitted by real-time observations. It always has a good correction on ionosphere delay, about 80%. Usually, the ionospheric delay extracted by UPPP contains the hardware delay deviation of the receiver and the satellite. The hardware delay will be constant during a specific period.

Lanyi used GPS observation data to extract STEC and gave a third-order polynomial model for ionospheric TEC modeling in 1988 [20]. The accuracy of modeled ionospheric TEC reached 1TECU using GPS. In 1993, JPL Lab proposed the triangular grid method to interpolate to establish a global ionospheric TEC model based on observation data of dozens of GPS monitoring stations distributed around the world and compared the results with spherical harmonics [21]. After 1998, IGS, CODE, JPL, UPC, ESA, NRCan, and other institutions submitted ionospheric product documents. In 2016, the Chinese Academy of Sciences (CAS/IGG) and Wuhan University (WHU) participated in IGS as ionospheric analysis centers. Table 1.1 shows the ionospheric modeling strategy of IGS IACCs.

In recent years, two-dimension ionospheric modeling based on thin shell models and empirical projection functions has been illustrated to have limited performance. New methods are proposed to reconstruct the 3D ionospheric electron density inversion technology, called ionospheric tomography. However, due to the small number of ground stations and inhomogeneous distribution, the amount of observation data is limited, which results in the tomographic result not being able to invert the electron density well. Over the years, two algorithms have been formed in ionospheric tomography. One is a non-iterative algorithm, which is using normalization, orthogonal algorithm, SVD, mixed reconstruction, and some other algorithms. In 2007, ESA proposed a method that is using the Chapman function as a basis, then integrating the ionospheric profile data obtained from the altimeter and GPS

occultation to realize 3D ionospheric modeling [25]. Jon Bruno performed spatial modeling based on the observations scanned by incoherent scattering radar (ISR) [26]. The other is an iterative algorithm represented by algebraic reconstruction. This method iteratively projects the GNSS rays on the hyperplane to obtain the electron density. Orhan et al. used Total Least Squares (TLS), Regularized Least Squares, Algebraic Reconstruction Technology (ART), and hybrid algorithms, and compared with the IRI model for 3D tomographic modeling [27]. Based on ART, Yuan Yunbin proposed to use the previous results to adjust the relaxation parameter vector to increase calculation efficiency [28].

Table 1.1 the ionospheric modeling strategy of IGS IACCs [22][23][24]

Agency	modeling method	Mathematic model	System
CODE	Global ionosphere modeling	Spherical harmonic function	GPS+GLONASS
ESA		Spherical harmonic function	GPS
JPL		Triangle mesh function+ Bicubic spline function	GPS
WHU		Spherical harmonic function	GPS
CAS/IGG	Inter-station area + Global ionosphere modeling	Generalized trigonometric series function + Spherical harmonic function	GPS+GLONASS
EMR	Distributed modeling site by site	tomographic function	GPS+GLONASS
UPC	Distributed modeling site by site	tomographic function	GPS
IGS	The weighted average of each analysis center		

1.4 Research goal and contents

1.4.1 Research goal

Recently, GNSS has developed quickly. The intelligence and automation of society have also increased requirements for positioning accuracy and convergence time. Moreover, the requirements for the accuracy of ionospheric models that affect positioning performance have also increased. This thesis focuses on the performance of PPP, extracting the slant total electronic content (STEC) based on the GNSS observations and modeling the ionospheric layer. The main purpose are listed as follows:

(1)The thesis builds a GNSS positioning algorithm platform to make the positioning results reach centimeter-level with 10-60min based on four navigation systems and compares the performance of four systems;

(2)The UPPP algorithm is used to extract ionospheric delay and estimates the performance of the ionospheric delays

(3)A single-layer VTEC model based on mathematical function is proposed to model the ionospheric layers and improve the positioning performance in the PPP algorithm.

(4)This thesis utilizes the tomographic algorithm to solve the single layer assumption's limitation and creates a three-dimension electronic density. Then, experiments verify the superiority of the algorithm.

1.4.2 Research contents

This thesis discusses the critical issues in the GNSS positioning and ionospheric inversion and the corresponding research goals. The main chapters are arranged in the following:

Chapter 1 introduces the background of PPP and ionosphere extraction and modeling researches in detail. Then, the critical issues unsolved are summarized. Finally, we conclude the research goals and the main research contents of this thesis.

Chapter 2 introduces the precise point positioning function models and statistic models. Then, the characteristics of the three models and the differences between them are summarized. Then we list the error source in the GNSS propagation and analyze what extent they affect and how to decrease their effects. American CORS data are process to implement the position based on four navigation systems and analyze their performance.

Chapter 3 introduces the basic features of the ionosphere in time and space distribution and their activities. Then, comparison among the typical ionospheric delay extracting methods are provided. Realize the ionospheric delay extraction method of the UPPP model.

Chapter 4 introduces the mathematic model and its feature, respectively. Then, we implement the algorithm based on the regional American CORS stations and use the PPP algorithm with the model constraints to verify the models' precision

Chapter 5 proposes a Tomography model and introduces its theory. Then, we implement the regional 3D electron density modeling based on the American CORS stations and verify the feasibility of the algorithm, analyze the differences and advantages with traditional methods.

Chapter 6 summarizes the main research work of the thesis. Then we propose the next step for future work.

1.5 Summary

This chapter introduces the background of PPP and modeling to explain why it is significant for research, introduces recent researches about PPP, ionospheric delays extraction, and ionospheric modeling. Then a summaries about the critical issues unsolved at present are gained. Finally, on this basis, the research goals and main research content of this thesis is determined.

2 Precise point positioning

This chapter will introduce some PPP functions: the IF PPP, the UofC PPP, and the UPPP model in Section 2.1. Also, in Section 2.2, some stochastic models are presented for calculating the weight of the GNSS observations.

Error models are also an essential part of PPP. We list the error source and how to solve it with the empirical models or available correction data in Section 2.3. PPP algorithm is designed based on the RTKLIB, improving the PPP performance. Then, the results of PPP using IGS stations' GNSS observations are shown and the differences between the four systems is analyzed.

2.1 PPP function

Code and carrier phase are the two basic GNSS observations. The code is measured by measuring the time a signal goes through from satellite to receiver, naming pseudo-range [1]. Usually, the noise of the pseudo-range is at the decimeter level. The carrier phase measurements are better, at about millimeter level. The variances of them are $0.3^2 m^2$ and $0.003^2 m^2$ respectively. Code and carrier phase measurement of two frequencies can construct the different PPP model.

2.1.1 IF PPP

Kouba et al. utilized dual frequencies to eliminate the effect of the first order of ionospheric delay by a linear combination, which is known as the traditional IF model [7].

$$\begin{aligned} P_{if,k}^s &= \frac{f_1^2}{f_1^2 - f_2^2} P_{1,k}^s - \frac{f_2^2}{f_1^2 - f_2^2} P_{2,k}^s \\ &= \rho_k^s + c\delta t_k - c\delta t^s + T_k^s + d_{k,P_{if}} - d_{P_{if}}^s + \varepsilon_{k,others}^s + \varepsilon_{k,P_{if}}^s \end{aligned} \tag{2-1}$$

$$\begin{aligned} \Phi_{if,k}^s &= \frac{f_1^2}{f_1^2 - f_2^2} \Phi_{1,k}^s - \frac{f_2^2}{f_1^2 - f_2^2} \Phi_{2,k}^s \\ &= \rho_k^s + c\delta t_k - c\delta t^s + T_k^s + b_{k,\Phi_{if}} - b_{\Phi_{if}}^s + \lambda_{If} N_{If} + \varepsilon_{k,others}^s + \varepsilon_{k,\Phi_{if}}^s \end{aligned} \tag{2-2}$$

Where,

$P_{if,k}^s$ is the pseudo-range of IF model;

$P_{1,k}^{s}$, $P_{2,k}^{s}$ is the pseudo-range receivers received based on different frequencies, L1 and L2;

$\Phi_{if,k}^{s}$ is the carrier phase measurement of the IF model;

$\Phi_{1,k}^{s}$, $\Phi_{2,k}^{s}$ is the carrier phase measurement receivers received at frequencies L1 and L2, respectively;

f_1, f_2 is the frequencies of L1 and L2, respectively;

ρ_k^s is the geometric distance between the satellite at the time of signal transmission and the receiver when the signal is received;

c is the speed of the light;

δt_k , δt^s is the receiver and satellite clock offset, respectively

T_k^s is tropospheric delay;

$d_{k,P_{if}}$, $d_{P_{if}}^{s}$ is the receiver and satellite hardware delay of pseudo-range, respectively;

$b_{k,\Phi_{if}}$, $b_{\Phi_{if}}^{s}$ is the receiver and satellite hardware delay of carrier phase measurement, respectively;

λ_{If} is IF wavelength.

$N_{If} = \frac{f_1^2}{f_1^2 - f_2^2}\lambda_1 N_1 - \frac{f_2^2}{f_1^2 - f_2^2}\lambda_2 N_2$, it is the ambiguity resolution of the IF model, which is equal to the combination of two frequencies' observations' ambiguity resolution;

N_1, N_2 is the ambiguity resolution of L1 and L2 respectively;

$\varepsilon_{k,P_{if}}^{s}$, $\varepsilon_{k,\Phi_{if}}^{s}$ is the noise of the pseudo-range and carrier phase.

$\varepsilon_{k,others}^{s}$ are the other errors that are not related to frequency, including earth rotation, relativistic effects, tide corrections, etc.

PPP usually eliminates the satellite orbit error and satellite clock error with precise ephemeris and precise satellite clock products. So the model above has eliminated those errors. The hardware delay deviation caused by the RF front-end and the signal processor has the same effect on the satellite signal of all channels on the same frequency, the receiver clock difference can absorb it during positioning [29]. Because ambiguity resolution will absorb the initial phase deviation of the satellite, it is not be considered this error in the float solution. The empirical models can fix some other errors irrelevant to frequency.

The unknown parameters that need to be solved are the receiver positions in ECEF, the receiver clock offset, the zenith tropospheric wet delay, IF ambiguity. These parameters can be estimated by the least square method (LSQ) and Kalman filter (KF). Also, for kinematic PPP, the receiver's speed and acceleration can help improve the solution.

2.1.2 UofC PPP

The UofC is developed by Gao (Calgary 2001), which utilizes the means of the code and carrier phase measurement [8] and combines with the IF PPP's carrier phase equation. The main idea shows in the following:

$$\begin{aligned} P^s_{UofC,k,1} &= \frac{1}{2}(P^s_{1,k} + \Phi^s_{1,k}) \\ &= \rho^s_k + c\delta t_k - c\delta t^s + T^s_k + \frac{1}{2}(d_{k,P_1} - d^s_{P1} + b_{k,\Phi_1} - b^s_{\Phi_1}) + \frac{1}{2}\lambda_1 N_1 + \varepsilon^s_{k,others} + \varepsilon^s_{k,P_{UofC}} \end{aligned} \tag{2-3}$$

$$\begin{aligned} P^s_{UofC,k,2} &= \frac{1}{2}(P^s_{2,k} + \Phi^s_{2,k}) \\ &= \rho^s_k + c\delta t_k - c\delta t^s + T^s_k + \frac{1}{2}(d_{k,P_2} - d^s_{P_2} + b_{k,\Phi_2} - b^s_{\Phi_2}) + \frac{1}{2}\lambda_2 N_2 + \varepsilon^s_{k,others} + \varepsilon^s_{k,P_{UofC}} \end{aligned} \tag{2-4}$$

Where,

d_{k,P_1}, d_{k,P_2} is the receiver hardware delay of different frequencies in pseudo-range;

$d^s_{P_1}, d^s_{P_2}$ is satellite hardware delay of different frequencies in pseudo-range ;

b_{k,Φ_1} , b_{k,Φ_2} is the receiver hardware delay of different frequencies in carrier phase measurement;

$b^s_{\Phi_1}, b^s_{\Phi_2}$ is satellite hardware delay of different frequencies in carrier phase measurement;

λ_1, λ_2 is the wavelength of the L1 and L2 respectively;

Others are the same as defined above;

The formulas 2-2, 2-3, and 2-4 made up the UofC model. As the function shows, the UofC model eliminates the effect of the ionosphere in GNSS propagation according to the criterion that the ionosphere delay has the characteristics of similar values and opposite signs in the code pseudo-range and carrier phase observations. But it cannot eliminate the Differential Code Bias (DCB) in satellite and receiver by Timing Group Delay (TGD) parameters from ephemeris or DCB correction broadcasted from IGS centers [30]. The noise of the UofC model is reduced by half compared with the raw observations, and the noise of the IF model is nearly three times larger than the raw observations.

2.1.3 UPPP

Traditional IF PPP and UofC PPP works through the combination of the pseudo-range and carrier phase to eliminate the effect of the ionosphere. However, this will lead to incomplete information. For solving this problem, Keshin et al. proposed the UPPP model based on raw observations [9]. In 2011, Zhang studied further to extract the ionosphere [19].

$$\begin{aligned} P^s_{j,k} &= \rho^s_k + c\delta t_k - c\delta t^s + T^s_k + \alpha_j I^s_k + d_{k,P_j} - d^s_{P_j} + \varepsilon^s_{k,others} + \varepsilon^s_{k,P_j} \\ \Phi^s_{j,k} &= \rho^s_k + c\delta t_k - c\delta t^s + T^s_k - \alpha_j I^s_k + b_{k,\Phi_j} - b^s_{\Phi_j} + \varepsilon^s_{k,others} + \lambda_j N_j + \varepsilon^s_{k,\Phi_j} \end{aligned} \tag{2-5}$$

Where,

α_j is the parameter of the ionospheric delay;

I^s_k is the ionospheric delay along with the sight between receiver and satellite at the frequency f_j;

The other symbol definitions are the same as above.

Also, $d_{k,P_j} - d^s_{P_j}$ is transferred as the following formula:

$$d_{k,P_1} - d^s_{P_1} = d_{k,P_{IF}} + \frac{f_2^2}{f_1^2 - f_2^2}(d_{k,P_2} - d_{k,P_1}) - d^s_{P_{IF}} - \frac{f_2^2}{f_1^2 - f_2^2}(d^s_{P_2} - d^s_{P_1}) \tag{2-6}$$

$$d_{k,P_2} - d^s_{P_2} = d_{k,P_{IF}} + \frac{f_1^2}{f_1^2 - f_2^2}(d_{k,P_2} - d_{k,P_1}) - d^s_{P_{IF}} - \frac{f_1^2}{f_1^2 - f_2^2}(d^s_{P_2} - d^s_{P_1}) \tag{2-7}$$

From the 2-6 and 2-7, the definition consists of two parts. The first one is the DCB of the receiver and satellite, which can be stated like this: $B_k = d_{k,P_2} - d_{k,P_1}$ and $B^s = d^s_{P_2} - d^s_{P_1}$. $d_{k,P_{IF}}$ is absorbed in the receiver clock error, reducing unknown parameters. $d^s_{P_{IF}}$ is included in the precision clock error of IGS and eliminated by clock error products. $\frac{f_2^2}{f_1^2 - f_2^2}(d_{k,P_2} - d_{k,P_1})$ and $\frac{f_2^2}{f_1^2 - f_2^2}(d^s_{P_2} - d^s_{P_1})$ will be absorbed by the ionosphere [30].

2.2 Stochastic model

The stochastic model is to evaluate the observations' quality, which contributes to weight the observations and accelerate finding the solution. The noise of the observations is related to the elevation and SNR.

2.2.1 Stochastic model about elevation

Usually, the form $\sigma^2 = f(E)$ state the stochastic models. Scholars have invented various stochastic models, the most popular models are the exponential function model(Barnes, 1998) and the sine or cosine function model(Bernese, GAMIT).

The exponential function model needs a standard deviation of observations near the zenith σ_0 and a reference elevation E_0 [31], the model is :

$$\sigma^2 = \sigma_0^2 \left(1 + ae^{-E/E_0}\right)^2 \tag{2-8}$$

Another one just needs two initial empirical parameters [32][33]. then,

$$\sigma^2 = a^2 + b^2 \cos^2 E' \text{ or } \sigma^2 = a^2 + b^2 / \sin^2 E' \tag{2-9}$$

2.2.2 Stochastic model about SNR

The receiver SNR is related to factors such as atmospheric delay error, multipath effects, antenna gain, and internal receiver circuits. It reflects the data quality of the observations to a

certain extent and can be used to measure the noise level of the observations. The famous model is similar to 2-8 (Liu, 2002) [34]:

$$\sigma^2 = \sigma_0^2 \left(1 + ae^{-\frac{S}{S_0}} \right)^2 \tag{2-10}$$

2.3 Error source in GNSS propagation

In section 2.1, we have known that various errors in GNSS propagation can interfere with the positioning results. Moreover, there are some process strategies to eliminate them, which will lead to a more accurate position result. In the following sections, they are introduced them in three aspects: how they produce, what extent they affect, and how to correct them.

2.3.1 Precise satellite orbit and clock correction

In terms of SPP, the broadcast ephemeris contains he satellites' information, where we can get information about satellite orbit and clock information. However, there is a large error in the calculated orbit information and the satellite clock offset in the broadcast ephemeris, which is not suitable for the PPP algorithm. So precise satellite orbit information and clock correction are essential. IGS is an international agency providing precise satellite orbit information and clock correction [35]. Table 2.1 shows the main products IGS provides.

The IGS products are updated every five minutes to fifteen minutes. But the GNSS observations are updated at a high frequency. So we usually use Lagrange interpolation to get the accurate satellite orbit and clock offset [1].

It takes approximately 70ms for the GNSS signal to travel from the satellite to the receiver, at the speed of light. So the transmission time T_{trans} is need to considered. We can correct this error with 2-11.

$$T_{trans} = t_{rece} - \frac{P}{c} - \delta t^s \tag{2-11}$$

Where, t_{rece} is the receiver receiving time. P is pseudo-range.

Table 2.1 Satellite ephemeris / Satellite Clocks [3]

Type		Accuracy	Latency	Update	Sample Interval
Broadcast	orbits	~100 cm	real-time		daily
	Sat. clocks	~5ns RMS			
		~2.5ns SDev			
Ultra-Rapid (predicted half)	orbits	~5 cm	real time	at 03, 09, 15, 21 UTC	15 min
	Sat. clocks	~3ns RMS			
		~1.5ns SDev			
Ultra-Rapid (observed half)	orbits	~3 cm	3 - 9 hours	at 03, 09, 15, 21 UTC	15 min
	Sat. clocks	~150ps RMS			
		~50ps SDev			
Rapid	orbits	~2.5 cm	17 - 41 hours	at 17 UTC daily	15 min
	Sat. & Stn. clocks	~75ps RMS			5 min
		~25ps SDev			
Final	orbits	~2.5 cm	12 - 18 days	every Thursday	15 min
	Sat. & Stn. clocks	~75ps RMS			Sat:30s
		~20ps SDev			Stn:5min

When the signal is transmitted, the Earth still rotates. In the following circumstance when the transmission time is fixed, we need to calculate the conversion between the satellite positions at the launching time and at the receiving time, which is also called the Sagnac effect. This error takes about 200ns, corrected by formulas 2-12, 2-13.

$$r_{\text{rcv}}^{\text{sat}} = R\left(\omega_E * \Delta t\right) * r_{\text{trans}}^{\text{sat}} \tag{2-12}$$

$$\Delta t = \frac{\left| r_{\text{trans}}^{\text{sat}} - r_0^{rcv} \right|}{c} \tag{2-13}$$

ω_E is the Earth's rotation speed. $r_{\text{rcv}}^{\text{sat}}$ and $r_{\text{trans}}^{\text{sat}}$ is the satellites' position at receiving and launching time. R is the rotation matrix along the Z-axis. r_0^{rcv} is the receiver's position. Δt is to calculate the transmission time in a geometric distance between the $r_{\text{trans}}^{\text{sat}}$ and r_0^{rcv} [36].

2.3.2 Relativity

The influence of relativity accounts for two aspects, time and transmission path. Because the pseudo-range is measured by the receiver's and satellite's atomic clock to calculate their difference. According to Special Relativity, the satellite's speed is much faster than Earth's rotation, which cause time bias. Relative correction caused by satellite orbit eccentricity is calculated [37].

$$\Delta t_r = -2\frac{r^{sat} \cdot v^{sat}}{c^2} \tag{2-14}$$

Also, the gravitational field can cause the GNSS transmission delay, about 2cm. Then we take it into account and correct the geometric distance by 2-15.

$$\delta_{rel} = \frac{2 \cdot \mu}{c^2} \ln \frac{\rho^{sat} + \rho^{rec} + \rho_{rec}^{sat}}{\rho^{sat} + \rho^{rec} - \rho_{rec}^{sat}} \tag{2-15}$$

μ is the gravitational constant, about $3986004.418 \times 10^8 m^3 / s^2$. ρ^{sat} and ρ^{rec} respectively represent the geocentric distance of the satellite and the geocentric distance of the receiver. ρ_{rec}^{sat} denotes the geometric distance between the receiver and satellite [7].

2.3.3 Satellite and receiver antenna phase center offset and variation

The satellite's position calculated by ephemeris is satellite centroid coordinates. But in the real process, the signal is launched by the satellite antenna. Then it brings the error about the coordinates of the antenna phase center. With the move of the satellite, the antenna will move to point towards the Earth [7].

Usually, The error are stated by phase center offset (PCO) and phase center variation (PCV). These two parameters can get from the IGS. The PCO is to calculate the precise satellite position. We need to define a satellite-fixed coordinate system with the satellite's centroid as the origin. Then, the phase center is converted by coordinate conversion. The PCV is to calculate the residue of pseudo-range and carrier phase measurement. It relies on elevation and azimuth. After reading directly, the PCV corresponding to the current nadir angle can be obtained by interpolation after the known nadir angle [38].

2.3.4 Phase wind-up

The signals GNSS transmits are right-handed circularly polarized(RHCP) signals. Therefore, the carrier phase observations obtained from the phase difference between the satellite and receiver signals depends on the relative position of the receiver's and the satellite's antenna. The mutual change of the antenna will cause the phase of the measured carrier to change, which is called phase wind-up, which can reach a cycle at most [39].

To reduce the effect,first, we calculate the significant dipole vector by 2-16, 2-17.

$$\vec{d'} = \hat{e}_x - \hat{p}\left(\hat{p}\cdot\hat{e}_x\right) - \hat{p}\times\hat{e}_x \tag{2-16}$$

$$_x\vec{d} = \hat{n} - \hat{p}(\hat{p}\cdot\hat{n}) - \hat{p}\times\hat{e} \tag{2-17}$$

Where,

$\hat{p}$ is the unit vector between the satellite and the receiver;

$\left(\hat{e}_x,\hat{e}_y,\hat{e}_z\right)$ is satellite-fixed coordinate system unit vector;

$\left(\hat{n},\hat{e},\hat{u}\right)$ is the local receiver unit vector;

$\vec{d'}$ and $\vec{d}$ are the effective dipole of receiver antenna and satellite antenna determined by $\left(\hat{e}_x,\hat{e}_y,\hat{e}_z\right)$ and $\left(\hat{n},\hat{e},\hat{u}\right)$ respectively.

Then,the carrier phase wind-up correction amount ω is gained:

$$\omega = \text{sign}\left(\hat{p}\cdot\left(\vec{d'}\times\vec{d}\right)\right)\arccos\left(\frac{\vec{d'}\cdot\vec{d}}{\left|\vec{d'}\right|\cdot|\vec{d}|}\right) \tag{2-18}$$

$\text{sign}\left(\hat{p}\cdot\left(\vec{d'}\times\vec{d}\right)\right)$ is used to judge the quadrant. $\arccos\left(\frac{\vec{d'}\cdot\vec{d}}{\left|\vec{d'}\right|\cdot|\vec{d}|}\right)$ is correction.

2.3.5 Site displacement

2.3.5.1 Solid tides

Solid tides are the deformation of the Earth because of the influence from the gravitational attraction forces of Sun, Moon, and some others planets. As a result, the reference point on the Earth will displace permanently and periodically. The displacement can be 30 cm and 50 cm in the vertical and horizontal directions, respectively.

Spherical harmonics can represent solid tides. 'Love' and 'Shida' state the degree and order of the spherical. In solid tides correction, they are correspond to the geographic location of the station and the tidal frequency. To get the accuracy of 5mm, we request to consider the effect of the Sun and Moon. A Second-degree tide and an additional altitude correction term can satisfy the request [1].

2.3.5.2 Polar tides

Polar tides are the periodic deformation of the crust caused by the instantaneous rotation axis of the Earth. The errors it caused are about 25mm in the vertical direction and 7mm in the horizontal direction. The Polar tides change at different times. It can make the position result more accurate. According to the corrected parameters from the IGS, the model is (2-19)

$$\begin{aligned}
\Delta\varphi &= -9\cos(2\varphi)\left[\left(X_{p\text{ole}}-\overline{X_{p\text{ole}}}\right)\cos\lambda-\left(Y_{p\text{ole}}-\overline{Y}_{p\text{ole}}\right)\sin\lambda\right]\\
\Delta\lambda &= 9\sin(\varphi)\left[\left(X_{p\text{ole}}-\overline{X_{p\text{ole}}}\right)\sin\lambda+\left(Y_{p\text{ole}}-\overline{Y}_{p\text{ole}}\right)\cos\lambda\right]\\
\Delta r &= -33\sin(2\varphi)\left[\left(X_{p\text{ole}}-\overline{X_{p\text{ole}}}\right)\cos\lambda-\left(Y_{p\text{ole}}-\overline{Y}_{p\text{ole}}\right)\sin\lambda\right]
\end{aligned} \tag{2-19}$$

The latitude and longitude correction of the station ($\Delta\varphi$, $\Delta\lambda$) changes with the variation of the pole coordinate $\left(X_{pole}-\overline{X_{pole}},Y_{pole}-\overline{Y}_{pole}\right)$ [40].

2.3.5.3 Ocean loading tides

Ocean loading tides are different from solid tides and polar tides. It is not requested all the time. In static PPP during a twenty-four-hour period or station far away from the ocean (about 1000km or more), we do not take it into account [7][40]. The ocean loading tides can lead to centimeter-level error.

2.3.6 Differential code bias

Differential code bias (DCB) is the hardware delay of the satellites and receiver causing the error in GNSS observations. It is eliminated this error in traditional IF PPP, but the error is a critical error source in the UPPP or SPP model [41]. Now IGS provides the DCB files of the four central navigation systems to correct the error directly. However, this file only provides the satellites' DCB. For receivers, errors of the receivers' DCBs are absorbed into the receivers' clock error and can be estimated when ionospheric constraint exists .

2.3.7 Tropospheric effects

The troposphere is the closest to the ground in the atmosphere, less than 20km. Also, this part can cause the refraction of the GNSS signal, called the tropospheric delay. Due to its neutral feature, the delay is not affected by system frequency. Wherefore, it is the reason why the delay cannot use the dual-frequency combination to eliminate.

The tropospheric delay consists of two aspects when processing. The first is called the static or dry delay, which is associated with the higher part of the troposphere. It accounts for the most influence of the total tropospheric delay, about 90%. And the other part is called the non-static water, also called the wet delay, which is associated with the lower part of the troposphere. It consists of most of the water vapor [1]. The dry delay is easy to model, but the wet delay cannot. The main factor is the irregularity of water vapor. Also, the tropospheric delay is associated with the transmission path and elevation. So the formula is 2-20.

$$T = Z_{dry} M_{dry}(Elev) + Z_{wet} M_{wet}(Elev) \tag{2-20}$$

Where $Elev$ is the elevation, Z_{dry} and Z_{wet} are zenith delay corresponding to the dry and wet delay, respectively. M_{dry} and M_{wet} are the corresponding mapping function.

Saastanoinen model can fit the dry delay part.

$$Z_{dry} = \frac{0.00227680P}{1 - 0.00266\cos(2\varphi) - 0.280 \cdot 10^{-6} h} \tag{2-21}$$

Where P is pressure, the unit is mill bar.

Usually, the popular mapping functions are Neal mapping function (NMF) [42], Vienna mapping function(VMF) [43], global mapping function(GMF) [44]. Due to the NMF and

VMF have some drawbacks, the popular method is GMF. And usually, the mapping function based on the temperature is.

$$m(E)=\frac{1+\dfrac{a}{1+\dfrac{b}{1+c}}}{\sin E+\dfrac{a}{\sin E+\dfrac{b}{\sin E+c}}} \tag{2-22}$$

Where a, b, c are the parameters depending on the temperature on ground, station latitude, station height. More details show in the following.

$$a=a_0+\mathrm{Acos}\left(2\pi\frac{DOY-28}{365}\right) \tag{2-23}$$

$$b=0.0029 \tag{2-24}$$

$$c=c_0+\left[\left(\cos\left(2\pi\frac{DOY-28}{365}+\Psi\right)+1\right)\frac{c_{11}}{2}+c_{10}\right](1-\cos\varphi) \tag{2-25}$$

Where, a_0 and A is the mean and season value. c_0, c_{10} and c_{11} are the value in table 2.3.

Table 2.2 c_0 c_{10} and c_{11} value

	c_0	c_{10}	c_{11}	Ψ
northern Hemisphere	0.0620	0.000	0.006	0
Southern Hemisphere	0.0621	0.001	0.006	π

The mapping works under the assumption of a symmetrical azimuthal atmosphere around the GNSS site. It can work for most situations. However, under the influence of local and regional climate and weather conditions, the atmospheric delay at a constant elevation angle will vary slightly with the azimuth direction. Gradient and the wet tropospheric delay need to be estimated together to achieve the highest precision positioning application. The gradient mapping function expression is as follows.

$$M_{gr}(Azi,Elev)=\frac{1}{\sin(Elev)\tan(Elev)+C}\left(G_N\cos(Azi)+G_E\sin(Azi)\right) \tag{2-26}$$

Where Azi and $Elev$ stand for azimuth and altitude, respectively. G_N and G_E are the north-south and the east-west direction. If the two are estimated independently, C is 0.0031 and 0.0007, but this method is challenging to use, usually only the total gradient C is estimated to be 0.0032 [1].

2.3.8 Cycle slip and clock jump

Usually, the cycle slip and clock jump can make centimeter-level or meter-level position error. The existence of cycle slip is usually manifested as discontinuity of observations, which will lead to a more massive error in the positioning and more convergence time of PPP. Thence, it is a specific error that is significant. The popular methods are Melbourne-Wubeena(MW) combination and geometry-free(GF) combination [48].

MW combination is an advantageous method in identifying cycle slips. The main idea is in 2-28.

$$\begin{aligned} N_{MW}^{i} &= \frac{\left(L_{WL} - P_{NL}\right)}{\lambda_{\mathrm{m}}} \\ \lambda_m &= \frac{c}{f_1 - f_2} = 0.86\mathrm{m} \\ &\begin{cases} \text{exist} & N_{MW}^{i} - m > a \cdot \sigma \\ \text{none} & \text{else} \end{cases} \end{aligned} \tag{2-28}$$

Where,

L_{WL} and P_{NL} are the wide-lane(WL) of the carrier phase measurement and narrow-lane(NL) of the pseudo-range;

λ_m is the narrow-lane wavelength;

m is the mean of N_{MW}^{i};

a is constant and σ is the std.

Geometry-free combination of the carrier phase measurement is another method that can cooperate with the MW combination for cycle slip detection. It uses the adjacent epoch error and compares it with a certain threshold to judge if there is a cycle slip.

The internal time scale of geodetic and navigation GNSS receivers generally uses relatively inexpensive quartz clocks, which are less stable than the high-precision atomic clocks on the satellite side. As the measurement progresses, the clock error of the receiver will gradually drift, resulting in the continuous accumulation of synchronization errors between the receiver's internal clock and GPS time. To keep the receiver's internal clock synchronized with the GPS time as much as possible, when the receiver clock error drifts to a certain threshold, most receiver manufacturers control the insertion of the clock jump to ensure that the synchronization accuracy is within a specific range. There are generally four types of receiver clock jumps. Their characters show in Table 2.3 [49].

Table 2.3 characters of clock jump

Type	Receiver clock	pseudo-range	Carrier phase
1	jump	continuous	continuous
2	jump	jump	continuous
3	continuous	jump	continuous
4	continuous	jump	jump

For the first and fourth types of clock jumps, because their pseudo-range and phase changes are the same, they can generally be estimated together with cycle slips. For the second and third types of clock jumps, the pseudo-range and phase change methods are different, which may cause During cycle slip detection, the mutation of the test volume is far greater than the cycle slip detection threshold.

There are roughly two modes of clock jump detection. One is based on the parameter domain. According to the previously estimated receiver clock error parameters, it is judging whether there is a clock jump by analyzing the change between the epochs; the other is based on observation range, by analyzing the continuity of observations to detect whether there is a clock jump. Since the second method is more time-sensitive, the second method is generally used [50].

2.3.9 Ionospheric effects

The ionosphere is at a height range from 60 to 20000km above the surface. There will be refraction in the ionospheric layer, causing group delay and phase advance. The ionosphere can lead to meter-level error. A broadcast model or Global Ionosphere Map (GIM) can correct the ionospheric effect. Users can gain the broadcast model’s parameters from navigation

ephemeris and use them to correct ionospheric delay in SPP. There are some popular models used for satellite systems, the Klobuchar model used in GPS, The BDGIM in BDS-3. For the Klobuchar model, it assumes that there is a thin shell model at the height of 350 km. This model contains eight parameters ($\alpha_0,\alpha_1,\alpha_2,\alpha_3,\beta_0,\beta_1,\beta_2,\beta_3$) receiving from the navigation ephemeris. The daytime correction mode is a simple cosine format, while the nighttime correction mode is a constant value of 5ns. The details of the model lists in the 2-27 [45].

$$\begin{aligned}
&\Delta\tau = \begin{cases} D + A\cos\left(\dfrac{2\pi\left(t-T_p\right)}{P}\right), \left|t-T_p\right| < \dfrac{P}{4} \\ D, \text{ others} \end{cases} \\
&D = 5\times10^{-9}\,s \\
&M = \begin{cases} \sum_{i=1}^{4}\alpha_i\left(\varphi_m\right)^i, A > 0 \\ 0, A \le 0 \end{cases} \qquad P = \begin{cases} \sum_{i=1}^{4}\beta_i\left(\varphi_m\right)^i, P > 72000 \\ 72000, A \le 72000 \end{cases}
\end{aligned} \tag{2-27}$$

Where T_p is equal to 50400. φ_m is the geomagnetic latitude. The Klobuchar model can fix about 50% error of the ionospheric delay.

Galileo uses the NeQuick model to correct the ionospheric effect. The NeQuick model is a 3D model, which is different from the Klobuchar model [5]. That is the reason that it is better than the Klobuchar model. It only needs three parameters to calculate the ionospheric delay and can fix 70% error [46]. Other models like BDGIM and NTCM-BC also decrease the effect of the ionosphere. Since of seldom use, we won't talk about it here.

Another method is the Global Ionospheric Map(GIM), which is calculated by continuous GNSS observation rather than an empirical model. IGS can provide GIM in IONEX format. Its spatial resolution is 5° in latitude and 2.5° in longitude. It is updated every two hours before 2015 and every hour after 2015. The accuracy of GIM is about 2-8TECU, and it is about 0.32-1.28 meters on the L1 frequency of GPS [47].

2.4 Error budget and positioning flowchart

The following table lists the error sources, their error levels, how to decrease their effect mentioned in chapter 2.3. After these errors are corrected, centimeter-level positioning accuracy can be obtained, which will also benefit accurate Ionospheric observations extraction.

Table 2.4 Error source and correction

Error sources	Effect	Compensated	Methods
Satellite orbit	~1.0m	~2.5 cm	Precise satellite orbit and clock offset
Satellite clock	~0.75 m	~2.25 cm	
Sagnac effect	~75 m	~mm level	
Relativistic effects	~up to a meter	~mm level	
Satellite PCV and PCO	~2 m	~cm level	IGS ANTEX
Receiver PCV and PCO	depends	Absorbed in receiver clock	
Phase wind-up	~2-4 cm (up to one-half cycle)	~mm level	Yaw-attitude model
Solid tides	~dm level	~mm level	IERS 2010
Ocean loading	~cm level	~mm level	
Polar tides	~cm level	~mm level	
Satellite DCBs	~m level	~0.1ns	IGS products
Receiver DCBs	~m level	Absorbed in receiver clock in IF combination	
Tropospheric effect	~2 m for ZHD	~mm level	Saastamoinen model
	~up to dm for ZWD	Estimated	Estimation
Ionospheric effect	~2-10 m for vertical delays	Depends	Corrected by model or GIM
		~cm level	Estimation

For the above introduction, the flowchart of PPP is shown in Figure 2.1. The input files are Precise satellite orbit file (.SP3), Precise satellite clock file (.ClK), Global ionospheric map file (.I), Differential code bias file (.DCB), Satellite and receiver antenna file (.atx), Polar tide file (.eop), Ocean loading tide file (.blq). We use LSQ to do a single point position, gaining the approximate coordinate. In this step, we also need to execute Receiver Autonomous Integrity Monitoring (RAIM) to exclude the abnormal observations. We use the specific model or available correction data to reduce the effect of the error sources. Also, the cycle slip and clock jump detection is important. The former steps are about the process of observations. Then, we gain the precise satellite orbits and clock offsets From IGS. After these preprocesses, we calculate the position and other unknown parameters by the KF.

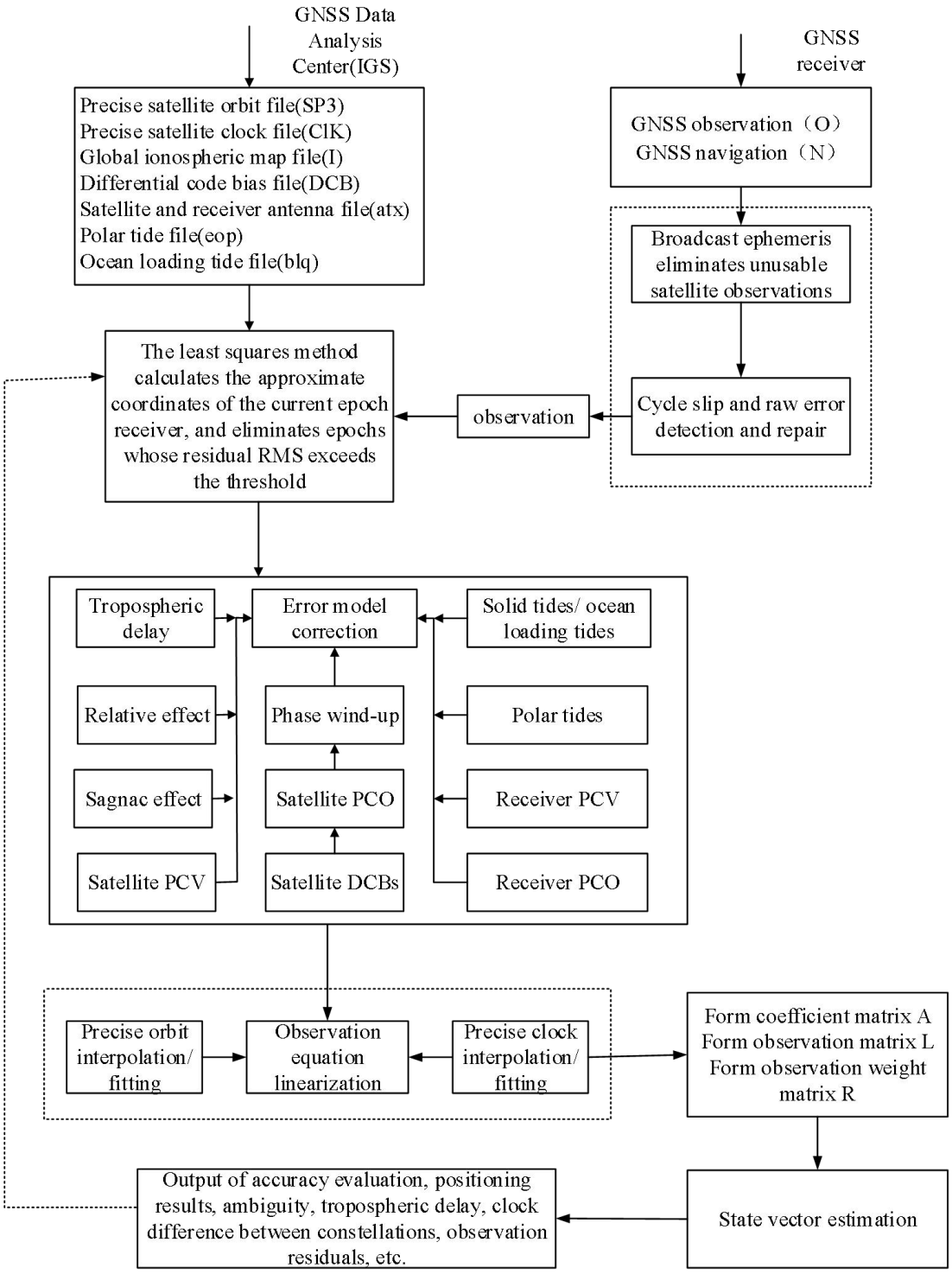

Figure 2.1 PPP flowchart

2.5 Experimental results and analysis

In this section, we designed the PPP algorithm based on the RTKLIB and improved the performance of the IF PPP, and focusing on the design of the UPPP. Using the GNSS

observations from the IGS Urum station on May 10th, 2020. The positioning algorithm is controlled according to the observation strategies in Table 2.5:

Table 2.5 Strategies of UPPP/IF

Model	UPPP/IF
observation	Raw GNSS data
Sample rate	The 30s for the static test
Cut-off angle	7°
GF threshold for cycle slip	0.1m
Satellite PCO/PCV	Igs.atx
Solid earth/tides	IERS 2010
Receiver clock	Random walk method
Troposphere	Saastamoinen model to solve dry delay and estimated wet delays
Ionosphere	estimated

First, the data quality analysis of GPS, GLONASS, Galileo, Beidou satellites, SNR, and DOP is compared. Then, every four hours as a set of data is used to reinitialize. Next, the convergence performance and positioning accuracy are compared. Finally, the feasibility of the algorithm is verified.

The GPS results shown in Figure 2.2. Figure 2.2(a) provide the visible period of GPS satellites on the day. Figure 2.2(b) shows that the visible number of GPS satellites is 7-12 and The average values of GDOP, PDOP, HDOP, VDOP are 1.7, 1.5, 0.8, 1.3. Figure 2.2(c) is about the measured SNR, multipath, elevation, and other parameters. The SNR range is about 30-55dB, the multipath influence is within two meters, and the SNR changes with the Elevation. The IF PPP can achieve the average convergence time of 39 minutes, and the convergence error is 0.01m, -0.004m, 0.025m according to Figure 2.2(d). The UPPP can achieve the average convergence time of 37.3 minutes, and the convergence error is 0.007m, -0.004m, 0.023m. For GPS, the UPPP method's performance is better than the IF method's, mainly in convergence time.

a)Visible period of GPS

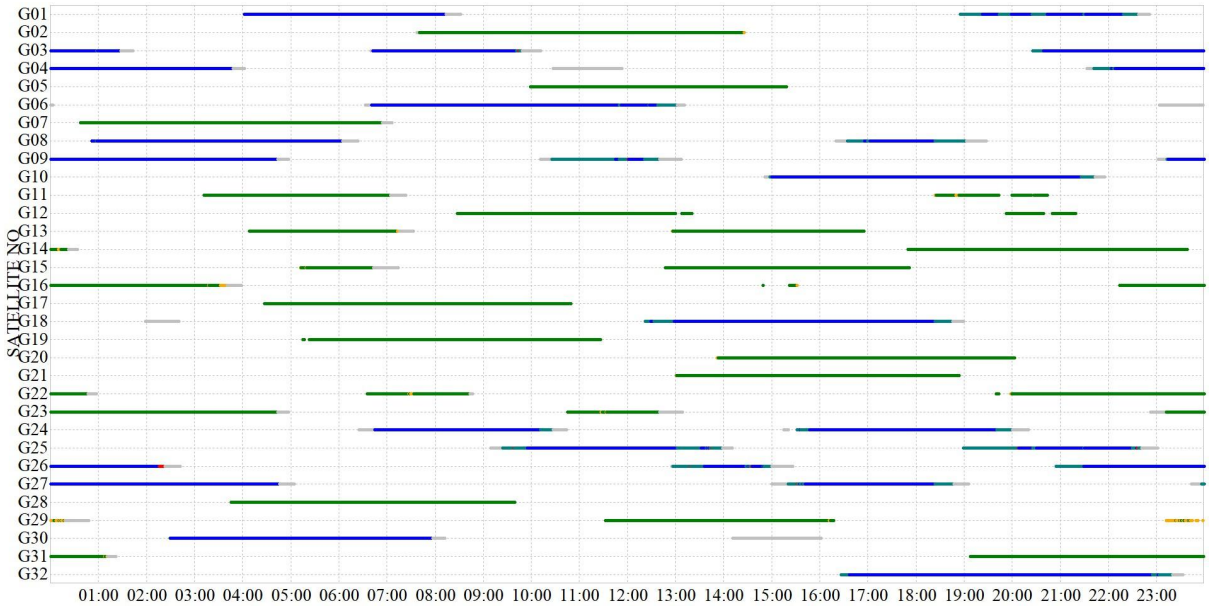

b)Visible number and DOP value of GPS satellites

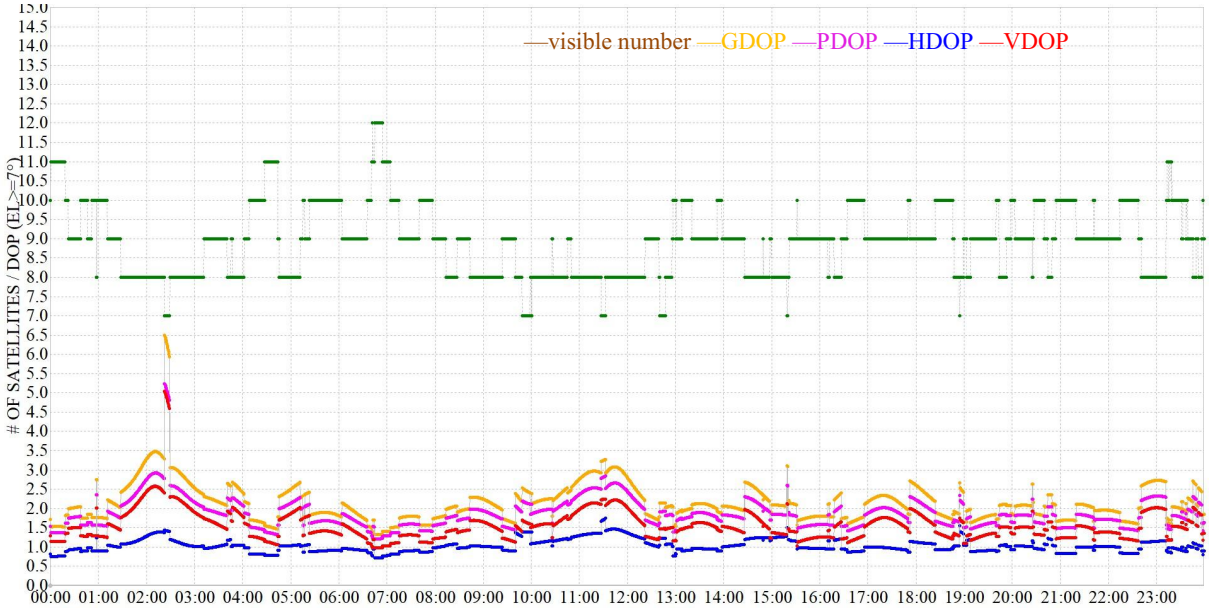

c)SNR, multipath, the elevation of observation of GPS observation

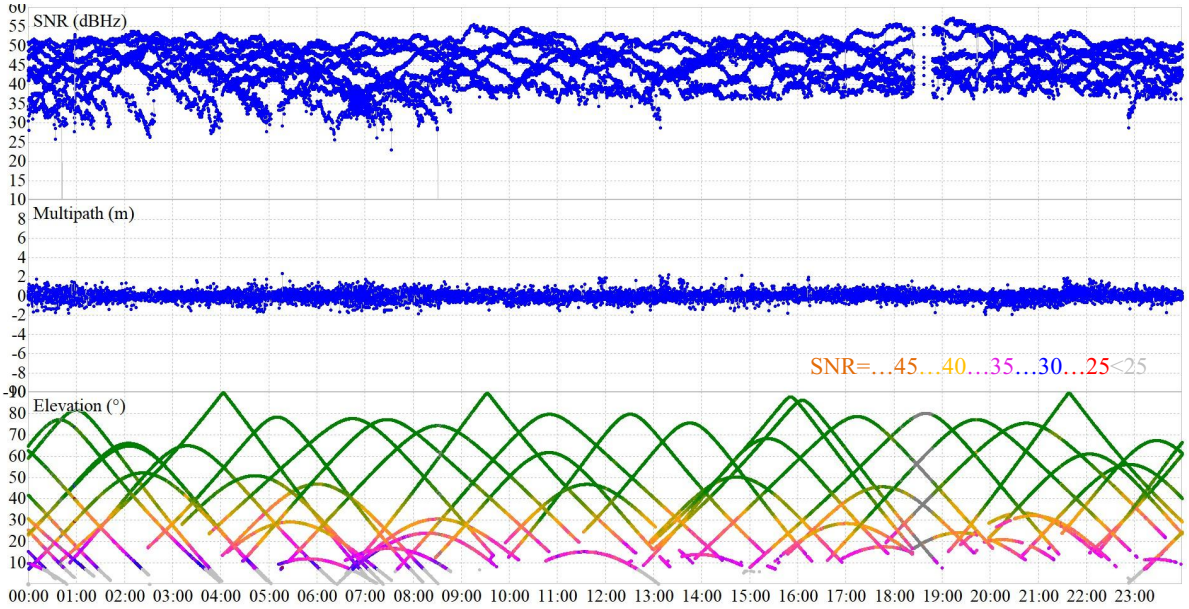

d)Positioning ENU error of GPS

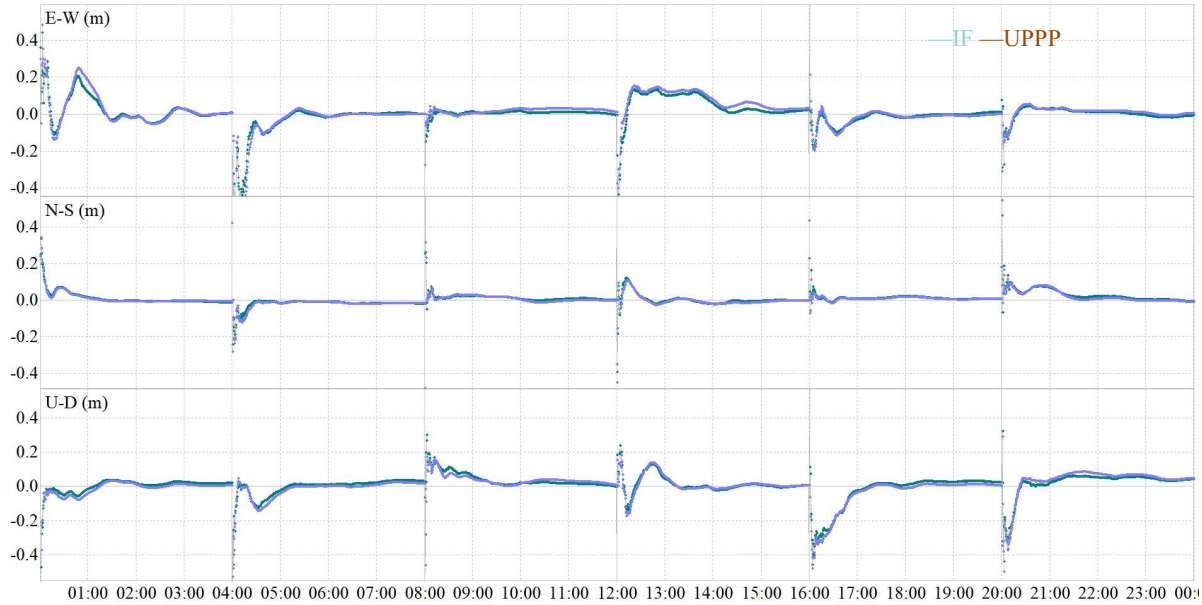

Figure 2.2 Performance of GPS. (a), (b), (c) is the analysis of the GPS observations. (d) shows the results with IF PPP and UPPP.

The performance of the GLONASS shown in Figure 2.3. Figure 2.3(a) provides the visible period of GLONASS satellites on the day. Figure 2.3(b) contains the visible number and DOP value of GLONASS satellites. The visible number is about 5-9 satellites. The average values of GDOP, PDOP, HDOP, VDOP are 2.7, 2.4, 1.3, 1.9, respectively. Figure 2.3(c) shows the measured SNR, multipath, elevation, and other parameters. The SNR range is about 30-55dB,

the multipath influence is within four meters, and the SNR changes with the altitude angle. The IF PPP can achieve the average convergence time of 45 minutes, and the convergence error is 0.011m, -0.004m, 0.036m according to Figure 2.3(d). The UPPP can achieve the average convergence time of 40 minutes, and the convergence error is 0.025m, -0.006m, 0.037m. Also for the UPPP and IF PPP, the conclusion is similar with GPS.

a)Visible period of GLONASS

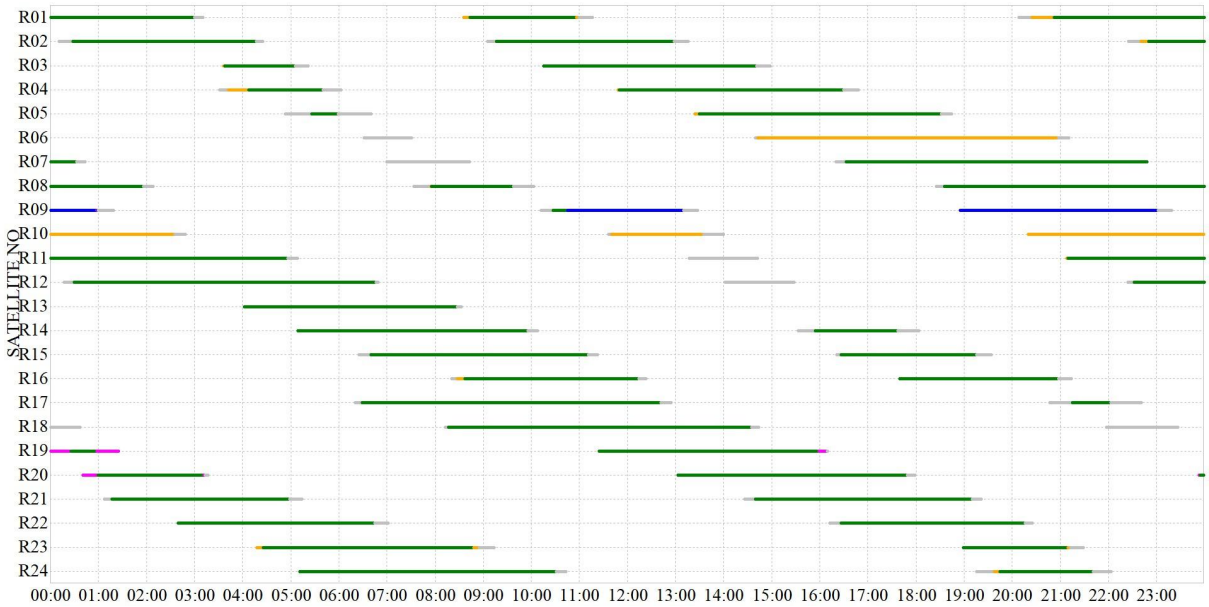

b)Visible number and DOP value of GLONASS satellites

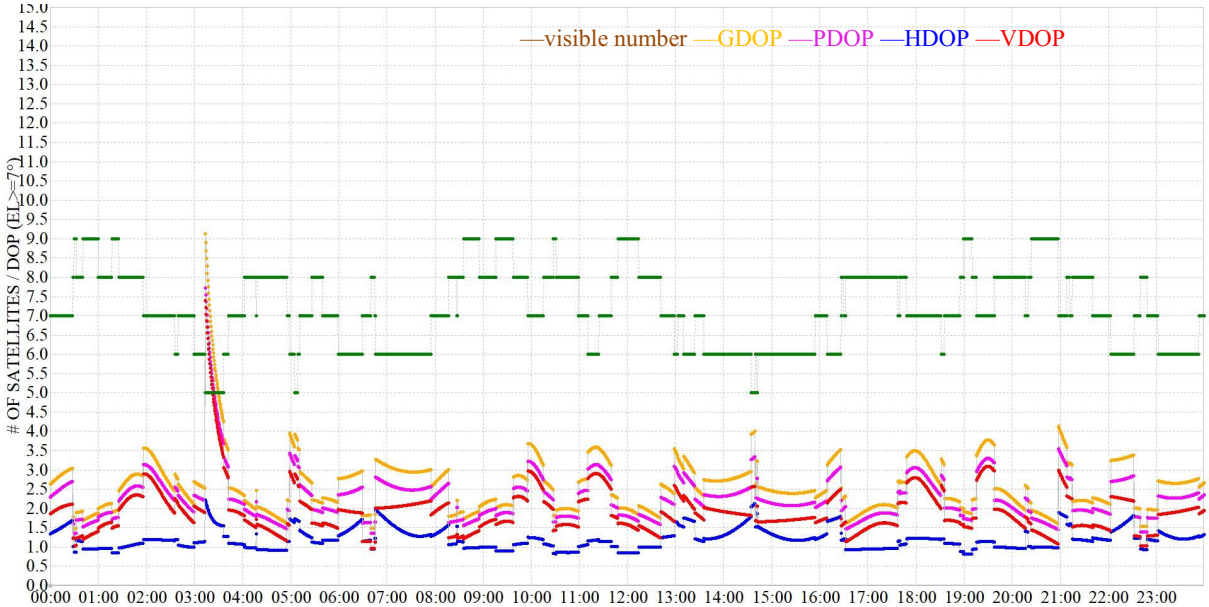

c)SNR, multipath, the elevation of observation of GLONASS observation

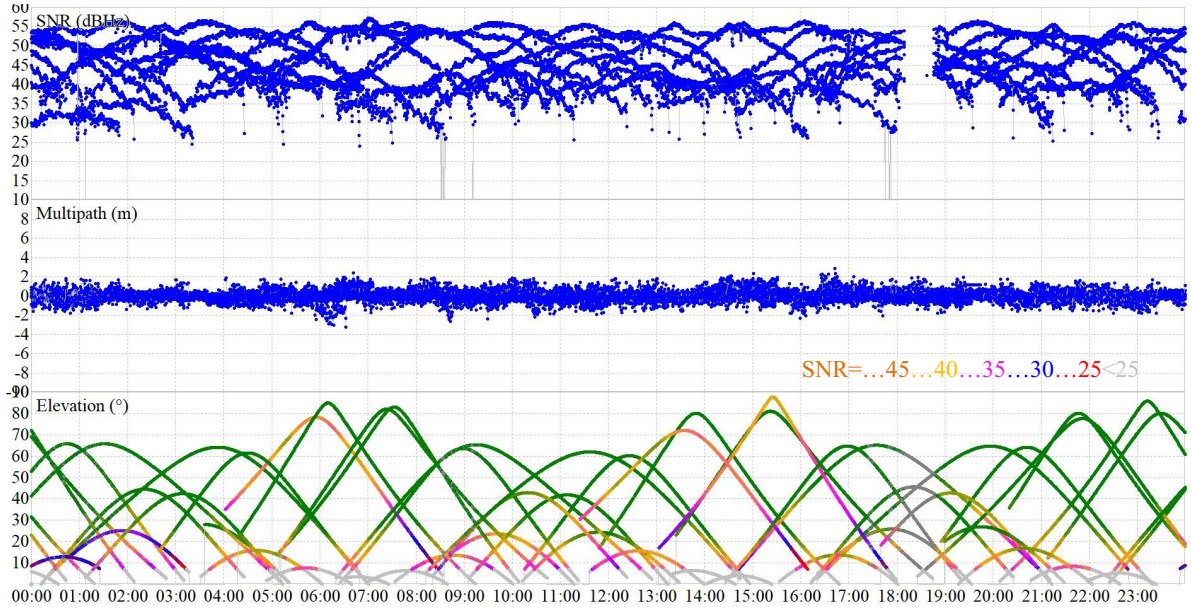

d)Positioning ENU error of GLONASS

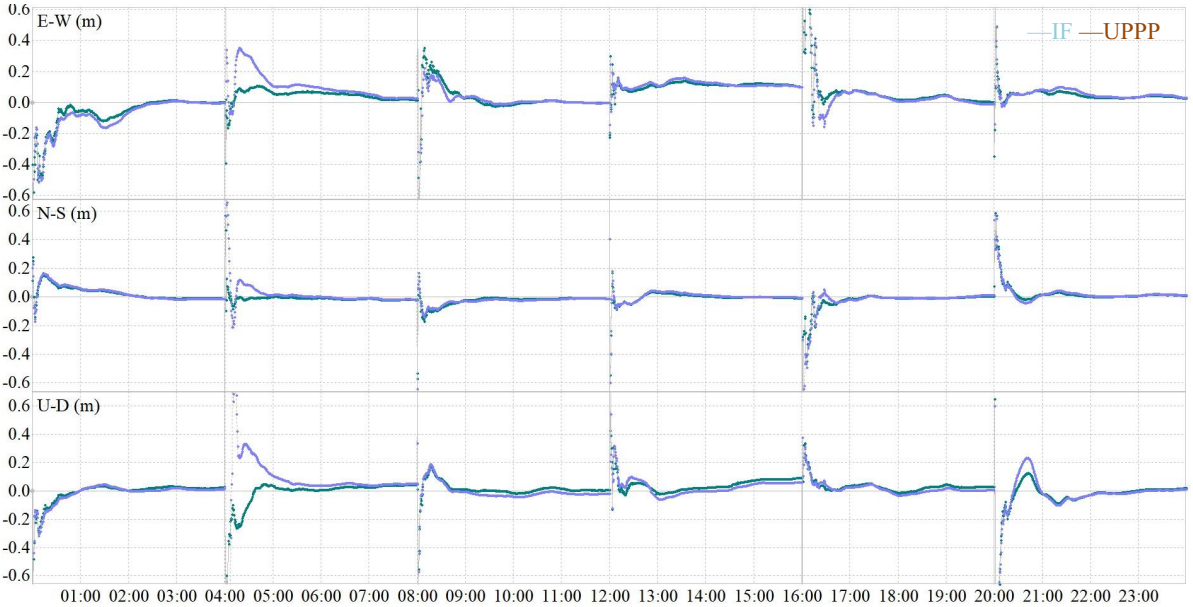

Figure 2.3 Performance of GLONASS. (a), (b), (c) is the analysis of the GLONASS observations. (d) shows the results with IF PPP and UPPP.

The results of Galileo is shown in Figure 2.4. Figure 2.4(a) provide the visible period of Galileo satellites on the day. It can be seen that the visible number and DOP value of Galileo satellites in Figure 2.4(b), about 4-10 satellites. The average values of GDOP, PDOP, HDOP, VDOP are 4, 3.0, 1.3, 2.7. Figure 2.4(c) shows the measured SNR, multipath, elevation, and other parameters. The SNR range is about 23-55dB, the multipath influence is within two meters, and the SNR changes with the altitude angle. In Figure 2.4(d), due to lack of the

visible satellites in Galileo, the DOP value is high, and the positioning convergence is not very good. Abnormal DOP or few obsevables will make the receiver not work. The UPPP model will be affected by the ionospheric delay, and the IF model will be better than UPPP model at some times.

a)Visible period of Galileo

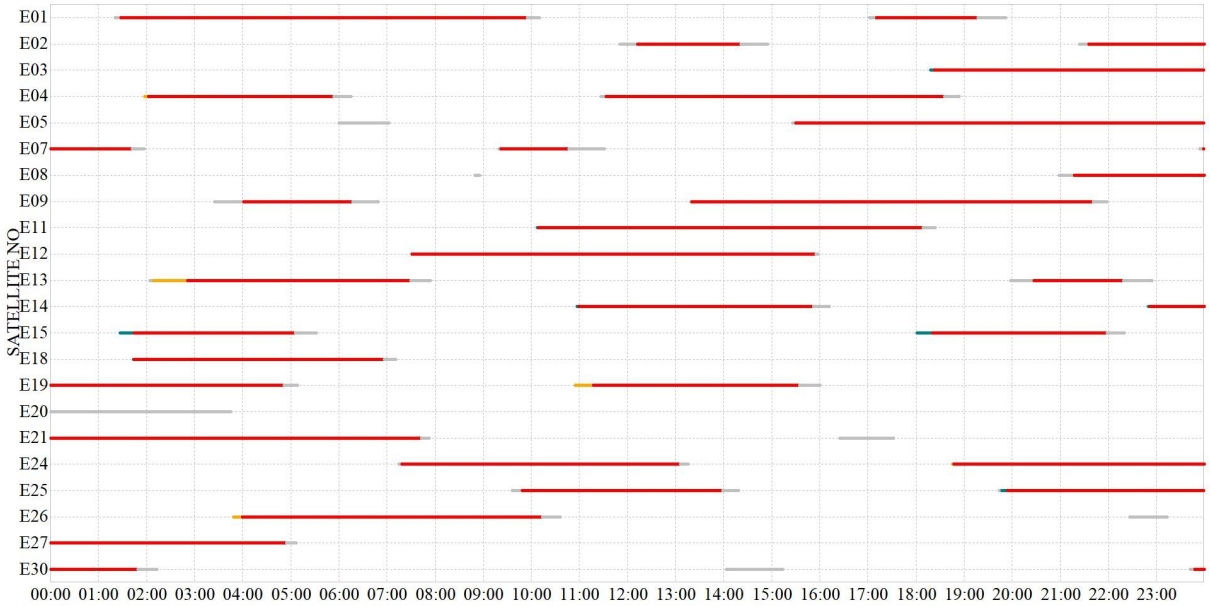

b)Visible number and DOP value of Galileo satellites

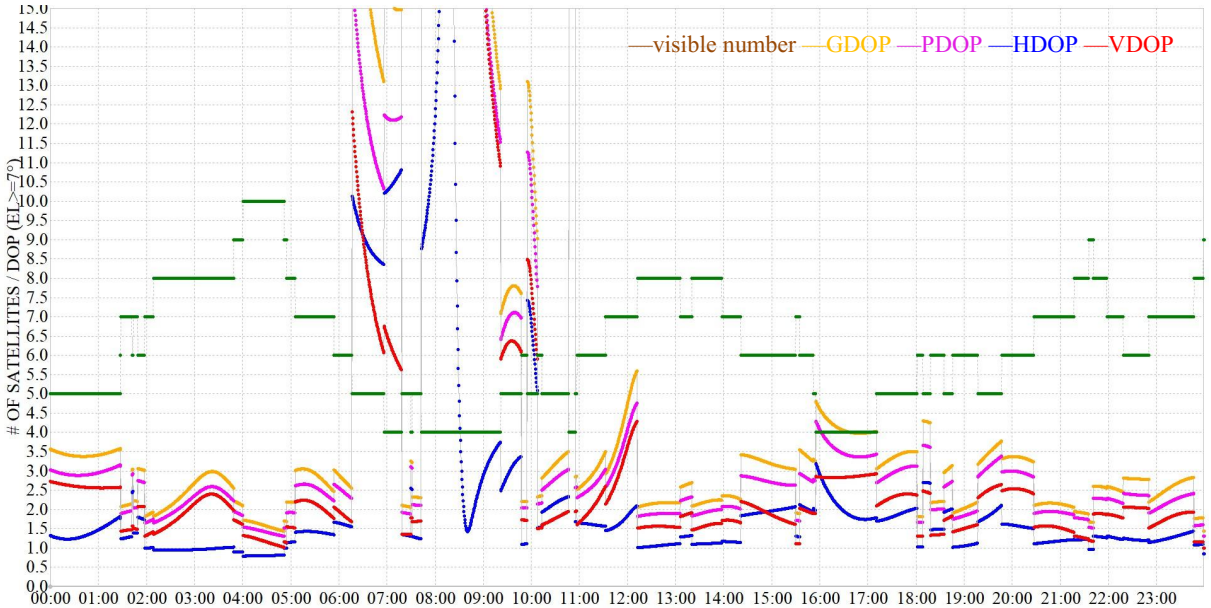

c)SNR, multipath, the elevation of observation of Galileo observation

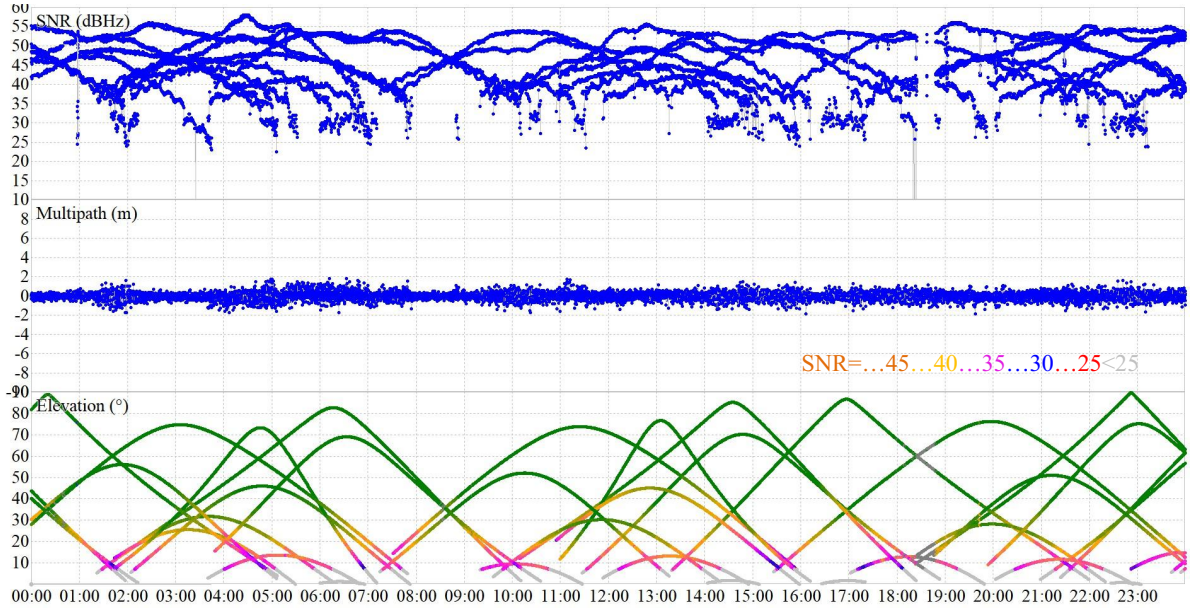

d)Positioning ENU error of Galileo

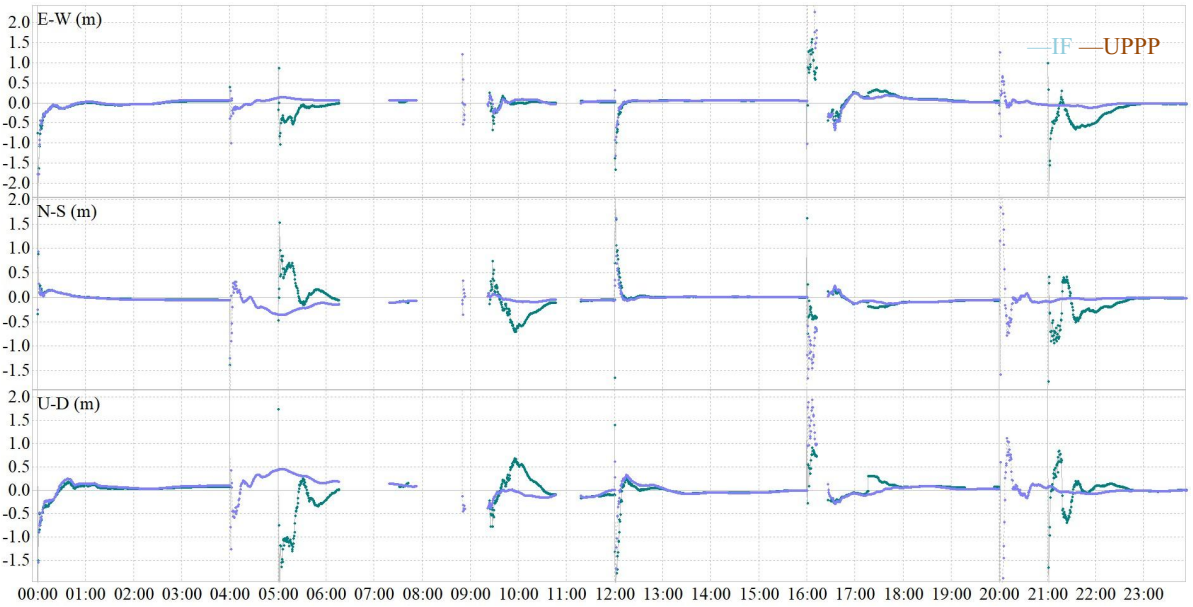

Figure 2.4 Performance of Galileo. (a), (b), (c) is the analysis of the Galileo observations. (d) shows the results with IF PPP and UPPP

Beidou's results are in the follows. Figure 2.5(a) shows the visible period of Beidou satellites on the day. Figure 2.5(b) shows the visible number and DOP value of Beidou satellites. The green line represents the visible number, which is about 13-18 satellites. The average values of GDOP, PDOP, HDOP, VDOP are 1.7, 1.5, 0.9, 1.1 respectively. Figure 2.5(c) shows the measured SNR, multipath, elevation, and other parameters. The SNR range is about 25-55dB, the multipath influence is within two meters, and the SNR changes with the altitude angle. The IF PPP can achieve the average convergence time of 62 minutes, and the convergence

error is 0.006m, -0.0256m, 0.0073m according to Figure 2.4(d). The UPPP can achieve the average convergence time of 60 minutes, and the convergence error is 0.002m, -0.0255m, 0.072m. For the UPPP and IF PPP, we can get the same conclusion with GPS and GLONASS. However, Beidou's performance is worse than GPS's even its visible satellites and DOPs are better.

a)Visible period of Beidou

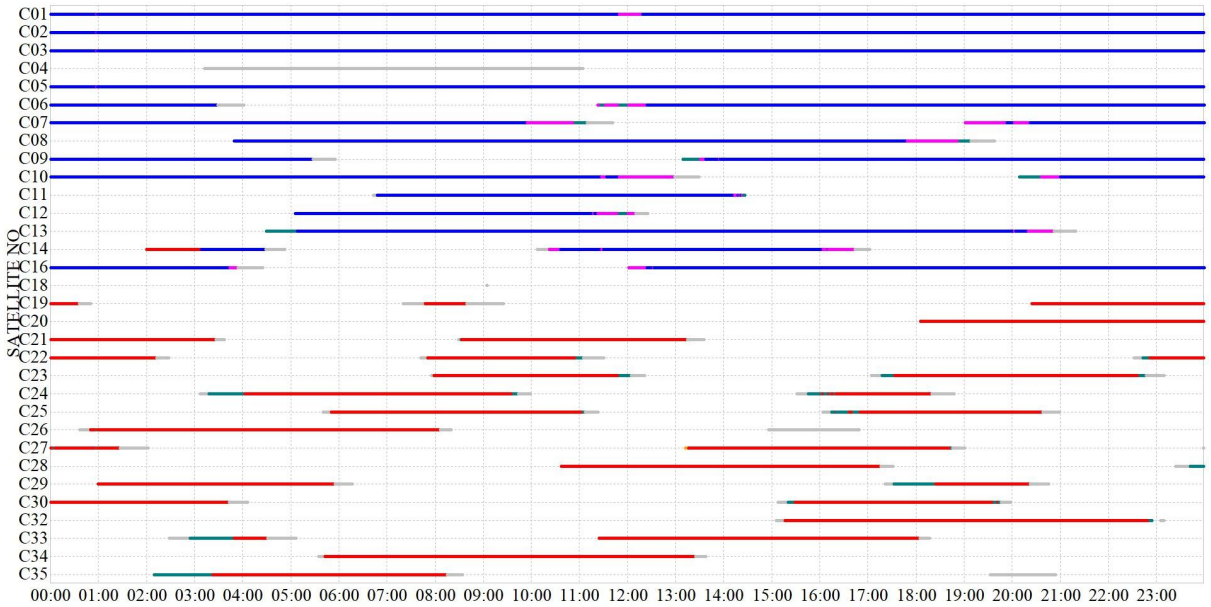

b)Visible number and DOP value of Beidou satellites

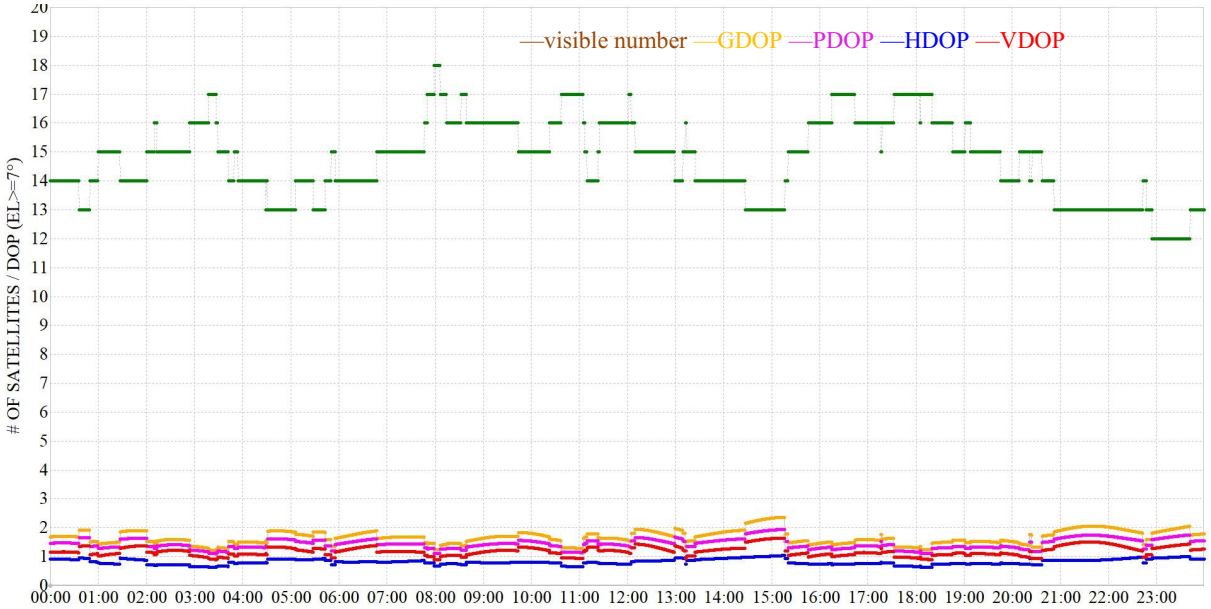

c)SNR, multipath, the elevation of observation of Beidou observation

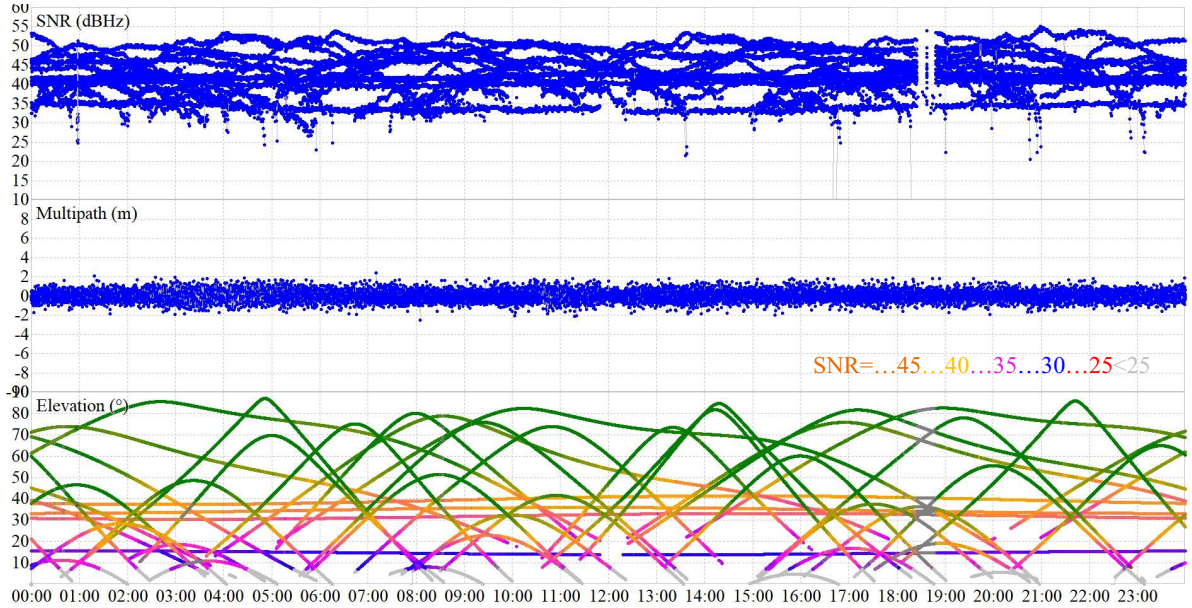

d)Positioning ENU error of Beidou

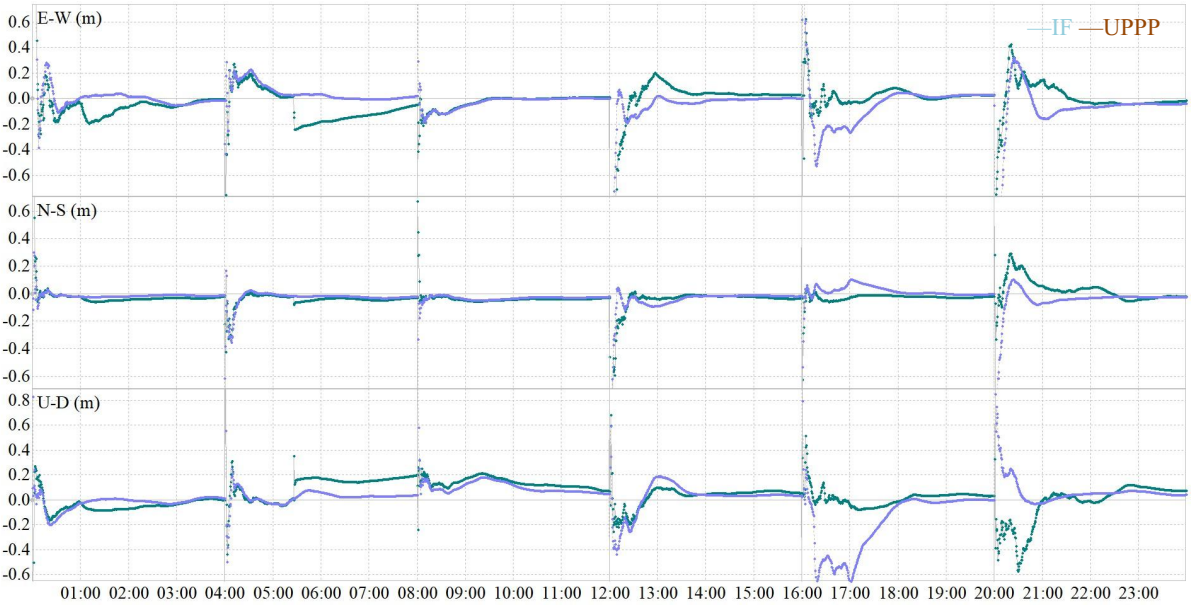

Figure 2.5 Performance of Beidou. (a), (b), (c) is the analysis of the Beidou observations. (d) shows the results with IF PPP and UPPP

At the same time, we use the combined positioning of GPS, GLONASS, and Beidou to verify the UPPP results further. It shows that the number of satellites has significantly increased, about 26-35. The fusion of the three systems has a better geometric position distribution than the single system. The values of GDOP, PDOP, HDOP, and VDOP are also apparently reduced, and their average values are 1.0, 0.9, 0.5, and 0.7, respectively. Figure 2.6 shows that

positioning performance has also improved. The average convergence time is 18.5min, and the ENU positioning error: 0.011m, -0.006m, 0.023m.

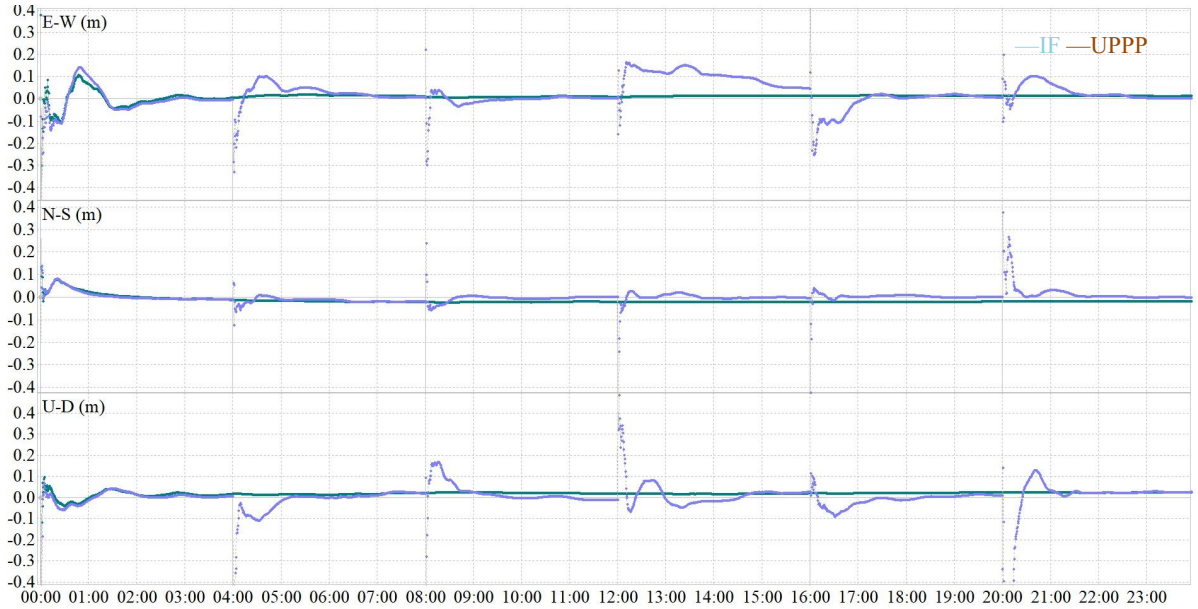

Figure 2.6 Performance of GPS+GLONASS+Beidou

From the data above, GPS and GLONASS have a good performance of PPP. Their position results are stable. The Beidou and Galileo are worse. The elevation of the satellite and DOP of the observation affects the performance of PPP. GPS, GLONASS, and Beidou have a better DOP and more observations than Galileo. It makes Galileo's position error large. When several systems used, the DOP will decrease, which means a better constellation geometric position distribution. Also, the use of several systems will increase the number of observations. As a result, the positioning error and convergence will improve.

To further verify the correctness of our algorithm, more observations of the station ABMF, URUM, GODS, DYNG, MATE, WUH2 are used. Figure 2.7 shows the stations' distribution. The statistic results of the positioning are shown in Table 2.6.

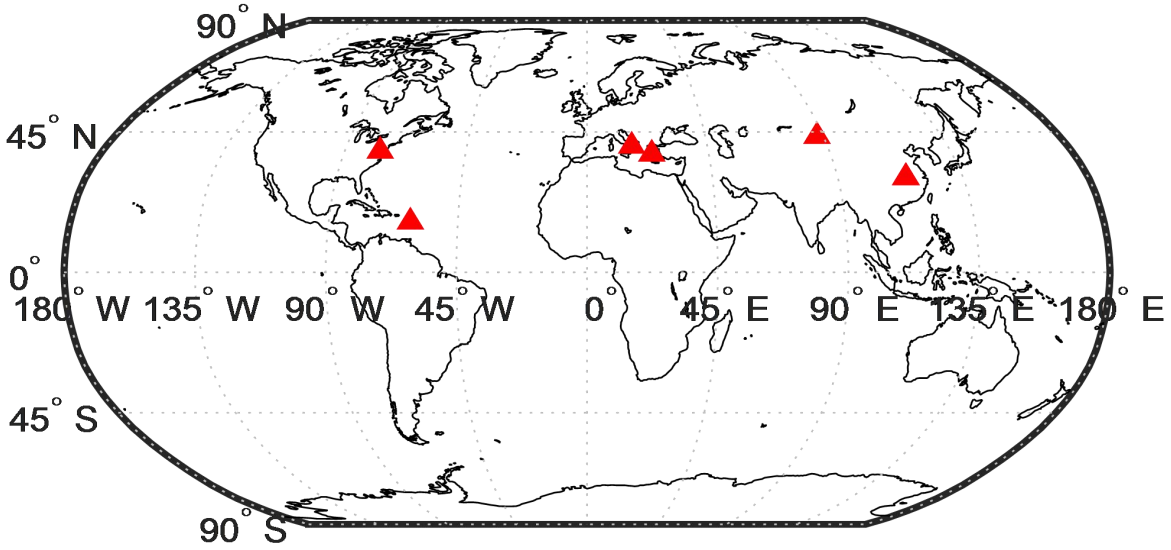

Figure 2.7 The distribution of IGS stations

Table 2.6 Statistical analysis of data results of UPPP results

	E/m	N/m	U/m	convergence time/min
GPS	0.032	-0.044	0.033	42
GLONASS	0.025	-0.006	0.037	38
Galileo	0.049	0.027	0.045	55
Beidou	0.05	-0.0623	0.0357	76
GPS+ GLONASS+ Beidou	0.020	-0.010	0.021	28

Table 2.6 is the average UPPP results of observations of the ABMF, URUM, GODS, DYNG, MATE, WUH2 on May 10th, 2020. That GPS's and GLONASS's positioning performances are similar, better than Galileo's and Beidou's. When we use GPS, GLONASS and Beidou together, the geometric position of the three systems, and the observations become more. The positioning performance will improve.

2.6 Summary

This chapter introduces three main PPP functions, IF PPP, UofC PPP, UPPP. We analyze the characters and differences among the PPP functions. IF and UofC PPP eliminates the ionospheric effect. Comparing to the IF, UPPP estimates the ionospheric delay and others. UPPP keeps all error sources in the signal propagation and avoids the impact of noise amplification and multipath errors caused by the combination of the GNSS observations. The stochastic model can be used to constrain and evaluate the observations when we estimate the solutions.

Also, this chapter introduces the error model we will use to improve the PPP's performance, analyzing the error before and after correction. Then, IGS station URUM's GNSS observations is used to analyze the performance of the IF PPP and UPPP algorithm. The UPPP model ensures that the average positioning convergence time is within 60 minutes, and the positioning error is within 10 cm, which is better than IF PPP. When using several systems, the position performance will improve, especially in the convergence time.

3 Ionospheric characteristic and extraction

This chapter is about ionospheric characteristics. It will describe how the ionosphere moves and its specific features in Section 3.1. Also, Section 3.2 introduces the propagation of GNSS signals in the ionosphere has a certain regularity. Then, section 3.3 shows the methods used to extract the slant total electronic content (STEC). Section 3.4 is about the experiment and discussion.

3.1 Ionospheric characteristic

The ionosphere is stratified into three layers, D, E, and F [51]. The D layer is the lowest and generates variations in the electronic density at sunrise and sunset. Its average electronic density is about 10^2-10^4/cm^3. The E layer is higher, about 90-140km. Its electronic density is higher than the D layer. For the F layer, we usually divide this layer into the F1 layer and the F2 layer. The F1 layer ranges from 140-200km whose electronic density is 10^{16}cm. The Chapman model can explain the E layer and the F layer. The electron density of the F2 layer accounts for the largest proportion in the ionosphere, which is the most concerned layer in ionospheric research. Usually, these four ionospheric layers are modeled. The activities of the ionosphere contain two aspects: regular variations caused by the large-scale changes and disturbances caused by sudden fluctuations in solar activities.

3.1.1 Regular variations

Regular variations in ionospheric are affected by the cycles of solar activity. Sunspots can represent solar activity. For a day's routine changes in the ionosphere, the maximum amount of electricity will be produced at 14:00 local time, and the ionosphere will have the greatest impact at this time. Also, the ionosphere has different electron densities in different seasons, which is called a seasonal anomaly. It usually shows that the amount of electricity at noon in winter is larger than that in summer. The reason for this phenomenon is mostly the high electronic recombination rate in summer [52].

We have already introduced the change characteristics of the ionosphere over time. Moreover, the spatial distribution also has a specific influence on the ionosphere. The geomagnetic field is essential for the formation of the ionosphere [53]. According to different latitudes and geomagnetic fields, the ionospheric region is divided into equator, mid-latitude and auroral (polar) regions. The equatorial region has the largest electron density and is susceptible to the

effects of ionospheric scintillation, causing equatorial anomalies. Mid-latitudes are the most stable, and mid-latitudes in the northern hemisphere are easy to model the ionosphere. The electron density in the aurora region will decrease significantly.

3.1.2 Disturbances

A disturbance that is very violent but not long-lasting (usually a few minutes to a few hours), it only occurs in the D layer of the ionosphere on the sunlit surface. Solar flares cause this disturbance. The intense far-ultraviolet radiation and X-rays emitted from the flare area reach the Earth after about 8 minutes, causing the Earth's sun-facing ionosphere, especially the electron density in the D layer, to increase suddenly [52]. This phenomenon is called sudden ionospheric disturbance. When this kind of disturbance occurs, the radio wave propagation state from VLF to VHF changes drastically [54].

Ionospheric disturbances generally last from several hours to several days. It can be divided into three stages. In the initial or normal phase, the electron density increases and reaches its peak or highest point, and lasts for several hours. In the negative phase, the previous peak electron density decreases and can last for several days. In the recovery phase, the ionospheric electron density returns to normal [52].

3.2 GNSS signals propagation in the ionosphere

The velocity of the GNSS signals in a vacuum is constant, about $3\times10^{8}\text{m/s}$. The speed will change caused by refraction when the signal enters the atmosphere. Then, we can get the refractive index of a medium (n) which is equal to the ratio of the speed of light (c) to the GNSS velocity in ionospheric medium (v) [55]. The formula 3-1 can calculate the atmospheric delay ($\delta\rho$).

$$\delta\rho = \int_{\text{Re}ceiver}^{Transmitter} n(l)dl - \rho = \int_{\text{Re}ceiver}^{Transmitter} (n-1)dl \tag{3-1}$$

This formula means integrating the path of each refraction (l) on the transmission path and subtracting it from a distance between the receiver and the transmitter (ρ) to obtain the atmospheric delay.

To calculate the total electron content (TEC) and the ionospheric delay or advance, we can integrate the transmission velocity [40]. Then the ionospheric geometric delays are obtained. The transmission differential of phase and code is as follows:

$$\begin{cases} l_{\phi,j} = -\dfrac{s_1}{f_j^2} - \dfrac{s_2}{f_j^3} - \dfrac{s_3}{f_j^4} \\ l_{g,j} = \dfrac{s_1}{f_j^2} + 2\times\dfrac{s_2}{f_j^3} + 3\times\dfrac{s_3}{f_j^4} \end{cases} \tag{3-2}$$

Where

$l_{\phi,j}$ and $l_{g,j}$ are the range propagation difference for carrier phase and code at frequency f_j respectively;

$s_1 = 40.309 \cdot \int N_e dl$;

$s_2 = 1.1284 \cdot 10^{12} \int B \cos\theta N_e dl$;

$s_3 = 812.42 \int N_e^2 d\rho + 1.5793 \cdot 10^{22} \int N_e B^2 \left(1 + \cos^2\theta\right) dl$;

B is the magnetic field intensity at the ionospheric pierce point (IPP) where the ray path from the satellite to the reference receiver intersects with the thin shell [47];

θ is the propagation direction's angle between the signal ray and the magnetic field at the IPP.

The first-order ionosphere accounts for 99.9% of the ionospheric delay and can produce meter-level errors, up to tens of meters. When the altitude angle is small, STEC can cause errors larger than 100 meters. Due to edge effects, the higher-order ionospheric term is ignored. The total electronic density can be calculated as follows [56]:

$$TEC = \int N_e dl \tag{3-3}$$

1 $TECU = 10^{16} el/m^2$. 1 $TECU$ is equal to 0.16 meters for the delay of GPS L1 and 0.27 meters for the delay of GPS L2.

3.3 STEC extraction methods

There are four common methods to extract the STEC, smooth code method, and PPP methods (IF model, UofC model, and UPPP model). The ionospheric observations are more accurate using PPP methods, compare to the smoothed code method.

3.3.1 Smoothed code

The code observation will be low quality, affected by the noise. Whereas, we need to calculate the ambiguity in the phase measurements. Using smoothed code can minimize the error of the code observation. This method also avoids resolving the ambiguity resolution. The critical steps are:(1) find a continuous arc;(2) compute the average of carrier phase measurement (Φ_3) and code (P_3); (3) correct the error [18]. This method's main idea is calculating the average value of a continuous arc and using the result to smooth the code. More details are in 3-4 to 3- 7:

$$P_3 = P_2 - P_1 = I_2 - I_1 + DCB^s_{P1/P2} - DCB^r_{P1/P2} + \sqrt{2}\varepsilon_P \tag{3-4}$$

$$\Phi_3 = \Phi_1 - \Phi_2 = I_2 - I_1 + B_I + DPB^r_{\phi 1/\phi 2} - DPB^s_{\Phi 1/\phi 2} + \sqrt{2}\varepsilon_\Phi \tag{3-5}$$

$$\langle \Phi_3 - P_3 \rangle_{arc} = 1/n \sum_1^n (\Phi_3 - P_3)_i = N_I + b^r_P + b^s_P + \langle \varepsilon_p \rangle \tag{3-6}$$

$$O_{smt} = \Phi_3 - \langle \Phi_3 - P_3 \rangle_{arc} = I_2 - I_1 + \left(DCB^s_{P_1/P_2} - DCB^r_{P_1/P_2} \right) + \langle \varepsilon_p \rangle + \varepsilon_p / time \tag{3-7}$$

Where

O_{smt} is the ionospheric observation in smoothed code method;

$\langle \ \rangle$ is the expectation algorithm;

ε_p is the multipath effect.

Although the smoothed code method can obtain the ionospheric delay conveniently and directly, it is hard for smoothed code methods to find a proper arc to decrease the effect of code noise [32]. Hence, the smoothed code method is not suitable for high accurate ionospheric modeling later.

3.3.2 PPP model

The PPP methods are different from the smoothed code method. It uses the function of PPP to extract the STEC. The results are much more accurate than the former methods.

The IF model and UofC method are based on the carrier phase measurement (Φ_3) and code (P_3). IF and UofC models can eliminate the ionospheric effect. Then, the ionospheric observations are recovered through the estimated ambiguity resolution. The basic idea is to find the proper parameter to replace the $\langle \Phi_3 - P_3 \rangle_{arc}$ in the smoothed code [57].

This thesis mainly discusses how to use the UPPP model to extract the ionospheric delays. According to 2-5, the ionospheric delays are estimated as unknown solutions. Then, ionospheric delays are extracted as the resolve positioning results using KF, epoch by epoch [19]. Then,

$$\begin{aligned} O_{UPPP} &= \left(\frac{f_1^2}{f_2^2} - 1 \right) \tilde{I}_1 \\ &= \left(\frac{f_1^2}{f_2^2} - 1 \right) \left(I_1 + \frac{f_2^2}{f_1^2 - f_2^2} \left(DCB^{S}_{P_1/P_2} - DCB^{r}_{P_1/P_2} \right) + \varepsilon_\Phi \right) n \\ &= I_2 - I_1 + \left(DCB^{s}_{P_1/P_2} - DCB^{r}_{P_1/P_2} \right) + \varepsilon_\Phi \end{aligned} \tag{3-8}$$

Where, O_{UPPP} are the ionospheric observations and $\tilde{I}_1$ is the estimated ionospheric observations.

Table 3.1 comparison between smoothed code method and UPPP

Method	Satellite clock	Observations' number	Unknowns' number	Freedom's number	Observations' variance	Biases
Smoothed code method	N/A	N/A	N/A	N/A	$\varepsilon_p / time$	DCBs Levelling error
UPPP	code clock	4n	3+1+1+3n	n-5	ε_Φ	DCBS

Table 3.1 shows a comparison between the smoothed code and UPPP. The table compares them in terms of six aspects such as the satellite clock, observations' variance, biases, and observations', unknowns', and freedom's number. The smoothed code method takes levelling

error into account. So, the ionospheric observations from UPPP are more accurate than the smoothed code.

3.4 Experimental results and analysis

We extract the ionospheric delays by smoothed code method and UPPP methods at the American CORS stations MOJC, MONE, MOMV on May 10th, 2020 and compare the results with the STEC simulated by GIM. Figure 3.1 show results.

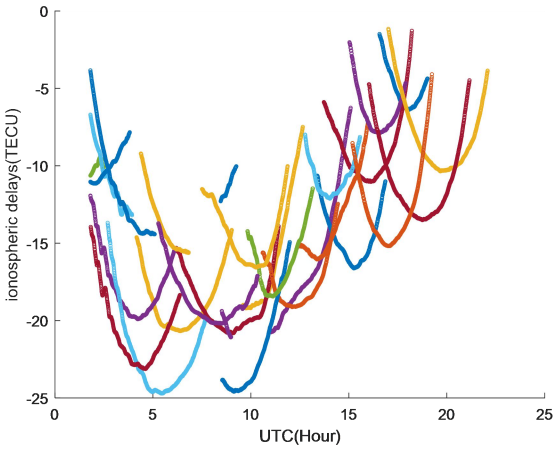

(a) MOJC: Ionospheric delay by smoothed code

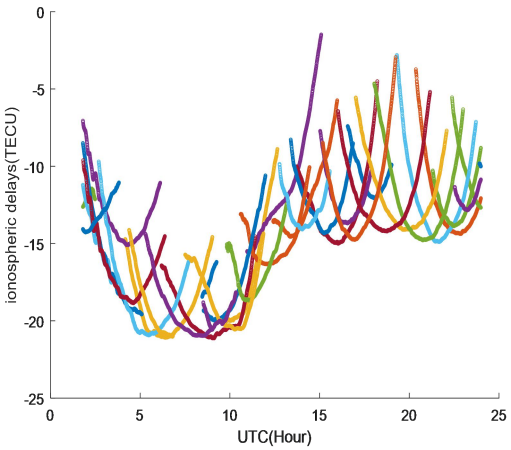

(b) MOJC: Ionospheric delay by UPPP

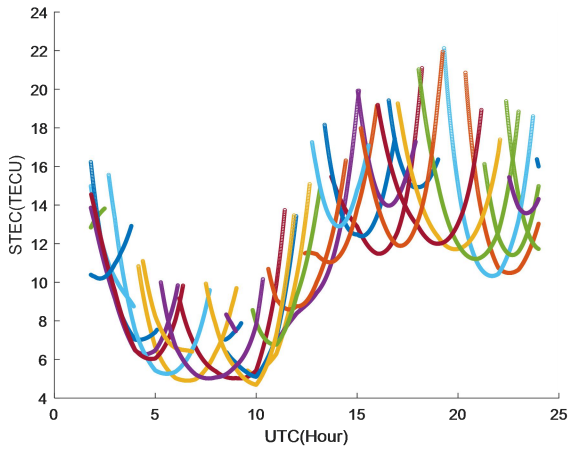

(c) MOJC: STEC by GIM

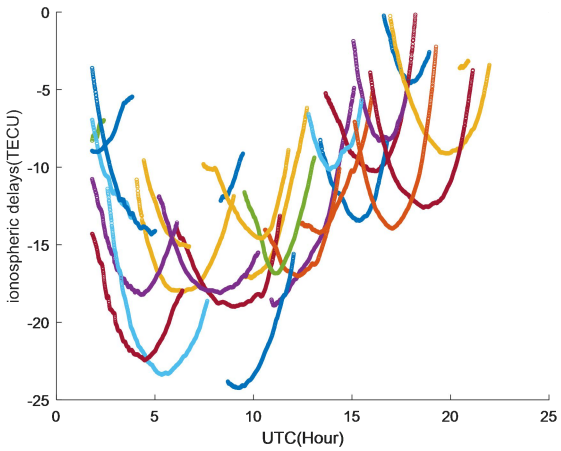

(d) MONE: Ionospheric delay by smoothed code

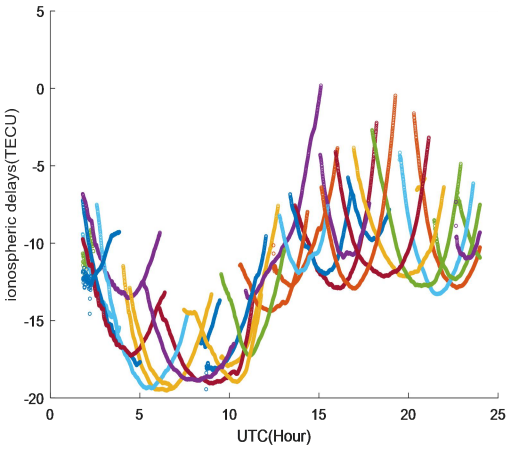

(e) MONE: Ionospheric delay by UPPP

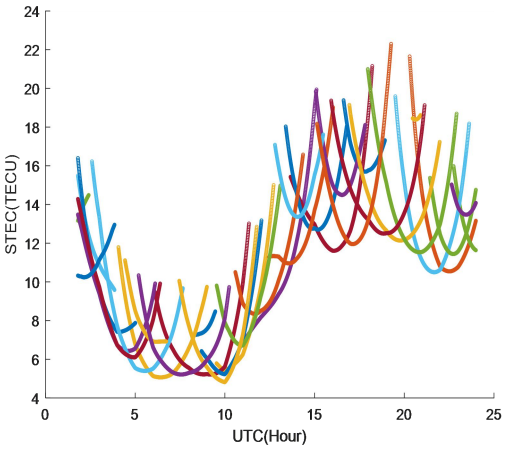

(f) MONE: STEC by GIM

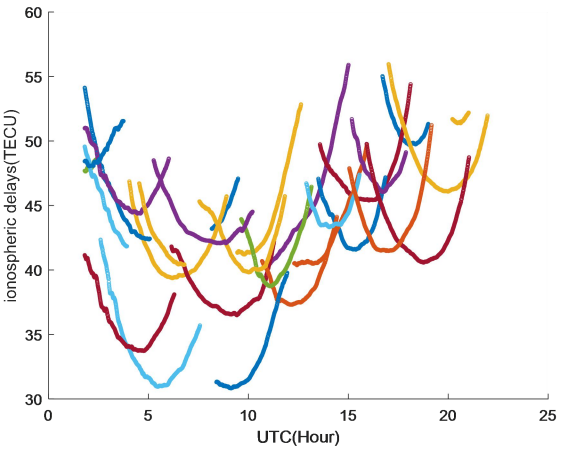

(g) MOMV: Ionospheric delay by smoothed code

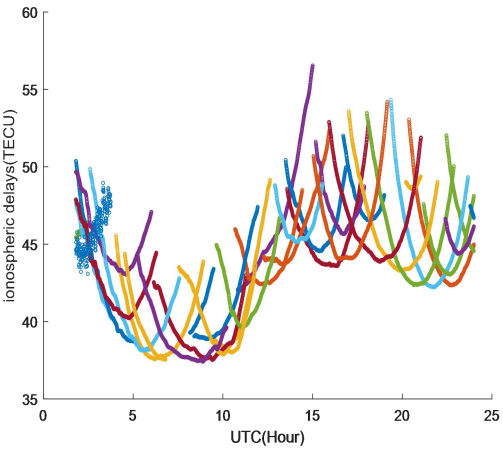

(h) MOMV: Ionospheric delay by UPPP

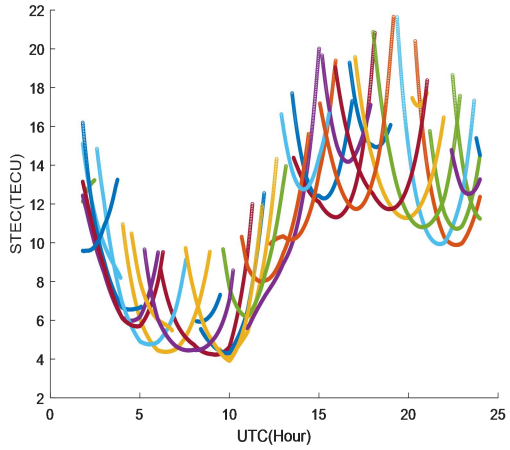

(i) MOMV: STEC by GIM

Figure 3.1 Estimated ionospheric delays of the MOJC, MONE, MOMV with UPPP model in 2020, May, 10th. The right hand, (a), (d), (g) is the corresponding ionospheric delay estimated by smoothed code, (b), (e), (h) is the corresponding ionospheric delay estimated by UPPP,(c), (e), (i) is the corresponding STEC simulated by GIM.

Due to the convergence may cost about 60min, the ionospheric delays will contain errors. So we use the ionospheric delays from 1hour to 24 hours. In Figure 3.1, each line means the ionospheric observations of the corresponding receiver when a satellite is moving. We conclude the ionospheric delay between satellites and receivers on May 10th, 2020. Figure 3.1 is the corresponding simulated results. In Figure 3.1, the actual observed value and the curve trend of the simulated STEC are relatively similar, but because GIM itself also has an error of 2-8 TECU, the curve is not the same. Due to the existence of the satellite and receiver DCB, the two curves have a relatively fixed deviation. And because the smoothed code needs to find the continuous epoch, so the number of ionospheric delays are less than the UPPP's.

3.5 Summary

In this chapter, ionospheric characteristics is analyzed about the time and space distribution characteristics. Also, regular variations and disturbances are common ionospheric activities. The regular variations are the predictable part of the ionosphere, whereas the disturbances are hard to predict. Due to media inconsistency, there will be refraction when the GNSS signals enter into the ionosphere. This phenomenon will also lead to changes in path and propagation speed. Ionospheric delay is a vital error source that affects the poisoning results.

Then, we list several methods that are commonly used and compare the smoothed code methods and UPPP methods. At last, we use the GNSS observable data of the MOJC, MONE, MOMV to extract the ionospheric delays using UPPP and compare them with the simulated value obtained from GIM.

4 Ionospheric modeling

As mentioned before, there are several applications model of the ionosphere. One is an empirical model, such as the IRI model, the NeQuick model. The other is forecast models such as Klobuchar, BDGIM. This chapter will introduce the traditional mathematical algorithm to model the ionosphere and analyze their features and differences in Section 4.1. Section 4.2 enumerates the common mapping function for mathematical modeling. Then, according to the observations of the American CORS on May 10th, 2020, we calculate the VTEC using a polynomial model and spherical harmonic function model, comparing them with the GIM in Section 4.3.

4.1 Mathematical model

For the ionospheric model, it is generally difficult for us to express it directly. Assuming that there is a "thin shell" on the outside of the Earth, we use mathematical models to characterize it. There are three common methods, polynomial model, trigonometric model, and spherical harmonic function model. We will introduce these three models and explain their characteristics.

4.1.1 Polynomial model

The polynomial model refers to the use of the Taylor expansion principle to express the regional site in a certain period as a polynomial function related to the geographic latitude of the precise ionospheric point (IPP) and the sun angle [58].

$$VTEC = \sum_{m=0}^{M}\sum_{n=0}^{N} E_{mn}(\varphi-\varphi_0)^m(S-S_0)^n \tag{4-1}$$

Where

E_{mn} is the unknown coefficient of the polynomial function;

N and M are the maximum orders of the polynomial function in latitude and longitude;

φ and φ_0 are the IPP and the center latitude;

λ and λ_0 are the IPP and the center longitude;

S , S_0 is the solar time angle where is the central point (λ,φ) of the observable region at the time t and t_0 , respectively;

Then, $S - S_0 = (\lambda - \lambda_0) + (t - t_0)\frac{\pi}{12}$.

Large amounts of studies have shown that the polynomial model has a simple structure, high computational efficiency, and superior performance. It can obtain high fitting accuracy in a small area and within a short time. However, the polynomial model is challenging to extend to a very high order because its function base is not orthogonal. So that global resolution may contain a large error.

4.1.2 Trigonometric model

We can also use the trigonometric series function to state the VTEC model. The formula shows below [59].

$$VTEC = a_1 + a_2 h + a_3 \varphi_{ipp} h + \sum_{i=2}^{7} \left\{ a_{2i} \cos[(i-1)h] + a_{2i+1} \sin[(i-1)h] \right\} \tag{4-2}$$

Where,

$a_i (i = 1,...15)$ are the unknown coefficients;

$h = \frac{2\pi(t-14)}{24}$ is the function of the local hour (t) of the IPP.

This model is designed according to the regulation in the ionosphere. That is during the day, the cosine changes with the local time (t), and generally reaches the maximum at 14:00. The difference is stable and relatively small at night, and the difference is not apparent with the local time. However, this model has a large fitting error.

4.1.3 Trigonometric model

Another mathematical model is a spherical harmonic function model, which was proposed by Schaer et al. in 1999 [58].

$$VTEC = \sum_{n=0}^{n_{\max}} \sum_{m=0}^{n} P_{nm}(\sin\phi)(A_{nm}\cos(m\lambda) + B_{nm}\sin(m\lambda)) \tag{4-3}$$

$$\phi = \sin^{-1}(\sin\varphi_M \sin\varphi_{IPP} + \cos\varphi_M \cos\varphi_{IPP} \cos(\lambda_{IPP} - \lambda_M)) \tag{4-4}$$

$$\lambda = \left(\lambda_{IPP} - \lambda_{SUN}\right) = \lambda_{IPP} + \frac{\pi}{12} \cdot (t - t_0) \tag{4-5}$$

Where,

$n_{\max}$ is the maximum degree of spherical harmonic expansion;

P_{nm} is the Legendre function with degree n and order m;

A_{nm}, B_{nm} are the unknown parameter;

λ_{IPP} and φ_{IPP} are the geographic latitude and longitude at the IPP;

λ_M and φ_M are the geomagnetic latitude and longitude;

λ_{SUN} is the meridian longitude through the centroid of the Earth and the sun.

Compared with polynomials, the spherical harmonic function model has a more complicated structure and calculation process. Still, it can better characterize the spherical characteristics of the ionosphere in a large area.

4.2 Mapping function

The VTEC is the vertical total electronic content. However, in real propagation, the transmit path is slant. The STEC is the integration of electron density along the propagation path [60]. Then,

$$\mathrm{STEC} = \int_{rev}^{sat} N_e \times dl = \sum_{i=1}^{m} \left(N_e\right)_i \delta l_i = \sum_{i=1}^{m} \frac{\left(N_e\right)_i \delta d_i}{\frac{\delta d_i}{\delta l_i}} = \sum_{i=1}^{m} \frac{\delta V_i}{\cos Z_i'} = \sum_{i=1}^{m} M_i \delta V_i \tag{4-6}$$

Where,

sat and *rev* are the satellite and receiver;

m is the number of layers;

i is the index of the current layer;

δl_i , δd_i are the slant and vertical height unit of the i^{th} layer;

$Z_i^{'}$ is the zenith distance at IPP of the i^{th} layer;

M_i is the mapping function of the i^{th} layer;

δV_i is the VTEC of the i^{th} layer;

The common assumption is that there is a single layer on the height of the Earth, which means that $n=1$. The mapping function is used to realize the conversion from VTEC to STEC.

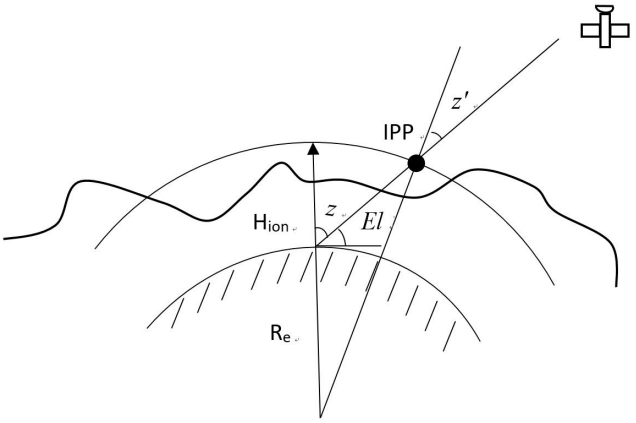

Figure 4.1 Scheme of the ionospheric SLM

According to Figure 4.1, we can express the single layer mapping(SLM) function as below:

$$MF = \frac{1}{\cos z^{'}} = 1/\sqrt{1-\sin^2 z^{'}} = 1/\sqrt{1-\left(\frac{R_e}{R_e+H_{ion}}\sin(z)\right)^2} = 1/\sqrt{1-\left(\frac{R_e}{R_e+H_{ion}}\cos(Elev)\right)^2} \tag{4-7}$$

R_e is the Earth's radius;

H_{ion} is the significant height of the SLM;

$z^{'}$ is the zenith angle at the IPP;

z is the zenith distance at a station along the LOS;

$Elev$ is the elevation at a receiver station.

Also, the modified single layer mapping (M-SLM) function is a method improved from SLM function.

$$MF = 1/\sqrt{1-\left(\frac{R_e}{R_e+H_{ion}}\sin(0.9782*(\frac{\pi}{2}-Az))\right)^2} \tag{4-8}$$

The formula 4-8 uses a coefficient of the zenith angle, about 0.9782 when the height is 506.7 kilometres.

According to the former discussion in Session 4.2, Session 4.3 and Session 3.3, we can conclude the formula as:

$$STEC_{obs} = \left(\frac{f_1^2}{f_2^2}-1\right)*\sum_{i=1}^{m} M_i \delta V_i + \left(DCB^s_{P_1/P_2} - DCB^r_{P_1/P_2}\right) + \varepsilon_\Phi \tag{4-9}$$

The $STEC_{obs}$ is the ionospheric delay extracted from the Smoothed conde method or UPPP. Others are the same as the definition above. The δV_i can be represented by the mathematic model. As a result, we can use the DCB file from IGS center to eliminate the DCB of the satellites and use the Kalman filter or Least Square method to resolve the model's parameters and the receivers' DCB.

4.3 Experimental results and analysis

For ionospheric modeling, multi-station fitting model results are better than the single station. The IGS stations are far away from each other, which is complicated for ionospheric modeling. We use the America CORS static stations. As we see in Figure 4.2, their latitude and longitude range is from 35^o to 41^o and from -95^o to -90^o respectively. So we use the data on May 10th, 2020. The stations' distance is about hundreds of kilometers. According to the stations' distributions, we set the spherical harmonic model's and the polynomial model's order to second. We extracted the STEC value by the UPPP method described in Chapter 3. Then, we choose the data from 1 a.m. to avoid the effect caused by the convergence. For high-quality data, we choose the GNSS observations whose elevations are lager than 30^o. Figure 4.2 is the stations' distribution.

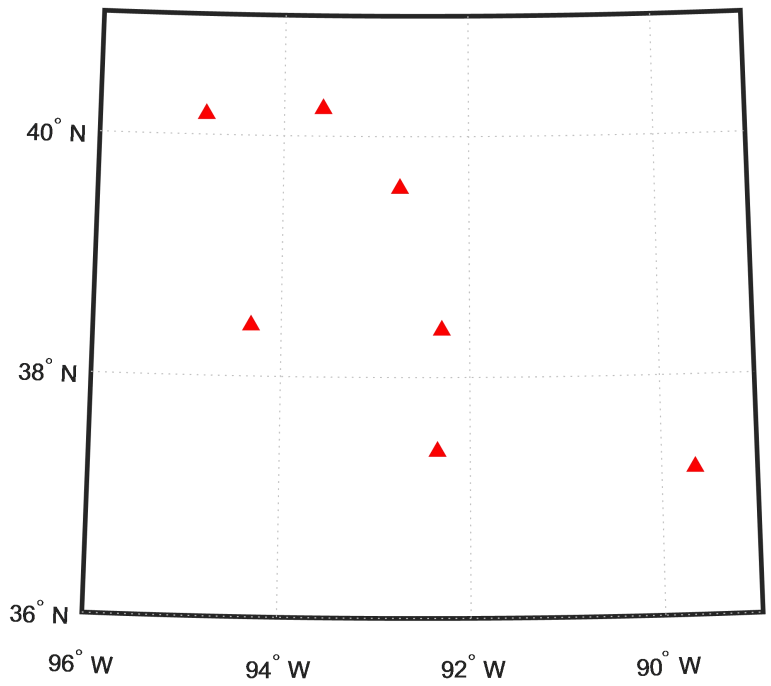

Figure 4.2 the USA CORS stations' distribution

Then we use the spherical harmonic model and the polynomial model to model the ionospheric. Figure 4.3 is the comparison between the VTEC value of one day and the GIM VTEC value under different modeling methods. It shows that these two models can represent the ionospheric activities. The changing trend is similar.

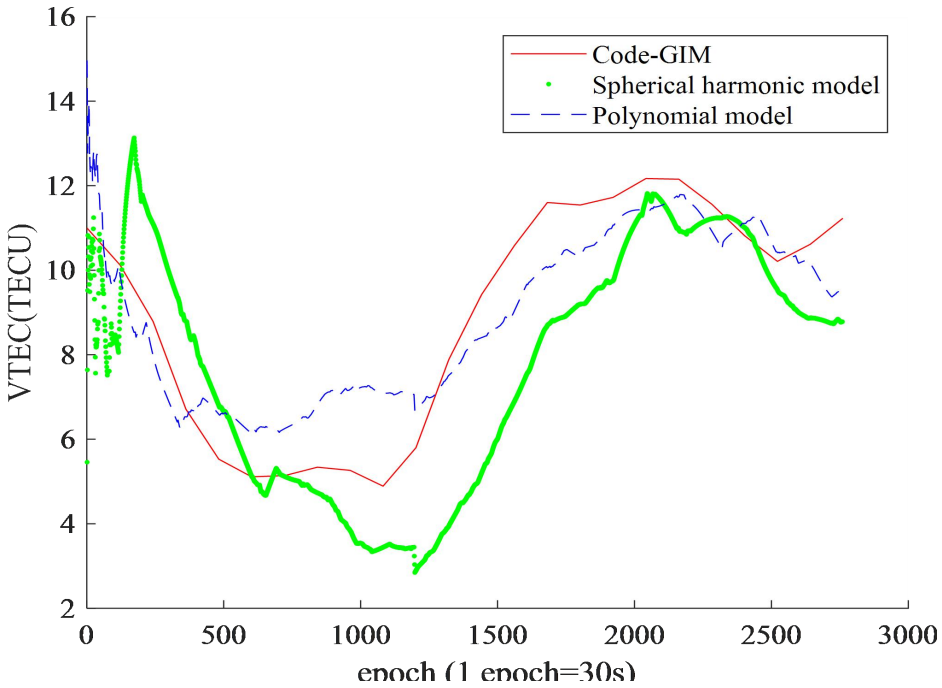

Figure 4.3 Comparison between the spherical harmonic model, the polynomial model, and GIM

However, GIM is not correct. The error is about 2 to 8 TECUs. So we need to illustrate the results using positioning. Figure 4.4 tells that when we use the modelled VTEC as the constrain, the accuracy of the position is better than using GIM. The convergence time of spherical harmonic model-constrain UPPP and polynomial model-constrain UPPP is both about 16.5 min, which reduces 2 min than using GIM as a constraint.

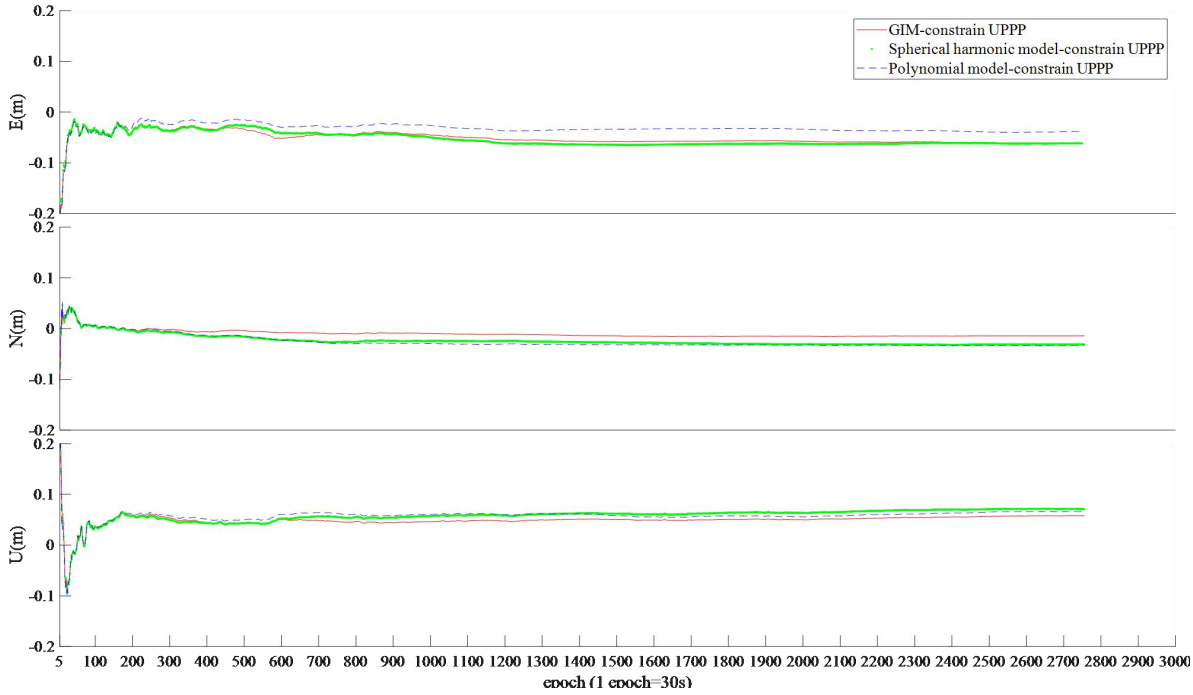

Figure 4.4 PPP position error based with ionosphere constraints based the VTEC reconstructed by two models and GIM.

4.4 Summary

This chapter introduces three mathematic models and analyzes their features. The polynomial model and the spherical harmonic function model are much more efficient. Then, we use the American CORS stations' GNSS observations to extract STEC, modeling the ionospheric layers. The results show that the modeled VTEC constraint can improve UPPP's performance and reduce the convergence time comparing the GIM VTEC constraint. The convergence time of the three directions of NEU is guaranteed to be within 60 minutes, and the convergence time is shortened by 10%.

5 Tomography model

In Chapter 4, we have known that the traditional model is single layers. According to 4-6, the model error will exist if we use a single layer. Because the accurate propagation consists of different refraction paths, the single-layer model does not represent the ionosphere well. In this chapter, we use CST to model the ionosphere. Section 5.1 introduces the theory of CST. We use the observations of American CORS sites on May 10th, 2020, to model the 3D electron density of the small area and analyze the results.

5.1 Compressed Sensing Tomography

This thesis proposed a method that is utilizing the ground stations' GNSS observations to reconstruct the ionospheric layer. The main idea is using the empirical model IRI or NeQuick as primary data, extracting the vital information as a basis by Principal Components Analysis, and using compressed sensing to reconstruct the three-dimension ionospheric electronic density.

5.1.1 Principal Components Analysis

Principal Components Analysis (PCA) is extracting the main feature of the main input matrix, weed out the noise and unimportant information through compress high-dimensional matrix to low dimensional. The main idea of PCA is finding the principal component of the largest difference in the data matrix. Usually, we calculate the covariance matrix, obtain the eigenvectors of the covariance matrix, select the k eigenvectors whose eigenvalues are large, and then form them into a matrix. In this way, we can transform the data matrix into low dimensions. Giving a data matrix $X_{N\times M}$, we get the foremost step in the following [61]:

(1) De-averaging (decentralization), that is, each feature minus its average, getting the new matrix A;

(2) Obtain the covariance matrix $Cov=1/M\bullet A^{T}A$, and calculate its eigenvectors and eigenvalues;

(3) Choose the k eigenvectors whose eigenvalues are large and construct them into the transform matrix $P_{N\times k}$;

(4) Get the final result: $Y=P^{T}X$.

By the steps above, we can get significant information from the primary data matrix, which will be beneficial to process the data.

5.1.2 Compressed Sensing

Compressed sensing, also known as compressed sampling (Candes, J. Romberg, T. Tao, 2004) is a method of processing limited data to reverse the original data from the limited data [62]. Compressed sensing needs to meet two prerequisites: sparsity and irrelevance. The specific meaning is that the input value needs to be sparse in a particular domain of transform and the observable matrix and the transform matrix are incoherent [63]. First, the original equation is:

$$Y = \Phi X \tag{5-1}$$

Where Y is the observations, X is the estimated solution and Φ is the observable matrix. Compressed sensing will transform the X into the sparse domain using a sparse matrix, getting Ψ, then $X = \Psi s$. The final formula is,

$$Y = \Phi \Psi s \tag{5-2}$$

Then, our question is changing from finding the proper X to s.

5.1.3 Compressed Sensing Tomography algorithm

In GNSS observations, there will be a ray path between each satellite and each station, which is also an ionospheric delay. As seen in Figure 5.1, a GNSS propagation ray will go through the ionospheric layer. According to 3-3, the STEC is equal to integrating the electron density on the transmission path. The ionospheric layer is divided into 3D grids with longitude, latitude, and height of 0.5°, 0.5°, and 50km, respectively. Assume that each grid's electronic density is homogeneous, STEC can be equal to the sum of the multiplication result of the path and the electronic density in each grid. The path can be separated in each grid, getting the observable matrix $B_{M,N_{\mathrm{lat}}\times N_{\mathrm{lon}}\times \mathrm{N}_{height}}$ and the electronic density grid $X_{N_{\mathrm{lat}}\times N_{\mathrm{lon}}\times \mathrm{N}_{height},1}$. M is the number of STECs, N_{lat} and N_{lon} is longitude and latitude grids' number, respectively. N_{height} is the number of grids in height. Then,

$$Y_{M} = B_{M,N_{\mathrm{lat}}\times N_{\mathrm{lon}}\times \mathrm{N}_{height}} X_{N_{\mathrm{lat}}\times N_{\mathrm{lon}}\times \mathrm{N}_{height},1} \tag{5-3}$$

Because the satellites' DCB is eliminated by available data from IGS and cannot ignore the receivers' DCB, the influence of the receiver's DCB should be eliminate by the single difference between satellites. The result is called dSTEC. We will calculate the dSTEC in the following step: After choosing a station (r3), we find the satellite with the highest elevation corresponding to the station, setting this satellite as the reference satellite (s3). Then, we subtract the reference satellite's (s3) STEC from other observation satellites' (s1, s2, s4) STEC at this site to get the STEC difference between satellites, also known as dSTEC.

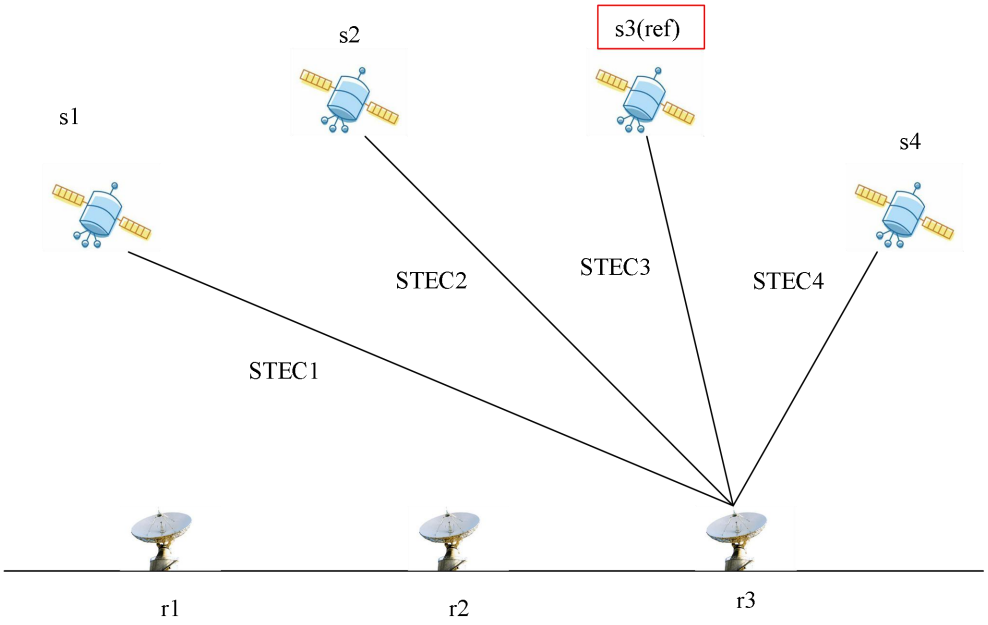

Figure 5.1 dSTEC calculation example

Then we get the dSTEC's formula:

$$dSTEC = Y_M^o - Y_M^{ref} = B^o_{M,N_{\text{lat}}\times N_{\text{lon}}\times \text{N}_{height}} X_{N_{\text{lat}}\times N_{\text{lon}}\times \text{N}_{height},1} - B^{ref}_{M,N_{\text{lat}}\times N_{\text{lon}}\times \text{N}_{height}} X_{N_{\text{lat}}\times N_{\text{lon}}\times \text{N}_{height},1} \tag{5-4}$$

From section 5.1.3, the sparse matrix Ψ is needed to transform $X_{N_{\text{lat}}\times N_{\text{lon}}\times \text{N}_{height},1}$. We use the IRI model to calculate this region's electronic density over a fixed period in the past, getting Ne_{prior} whose rows' and columns' number are A and $N \times N \times H$. Then PCA is to extract k significant grids, $Ne_{k,N_{\text{lat}}\times N_{\text{lon}}\times \text{N}_{height}}$.

Then, the compressed sensing theory and convex optimization are set to solve the problem by setting the objective function [64].

$$s = \arg\min\left\{\left\|Y_{dstec} - B_{dstec} \bullet \Psi \bullet s\right\|_2^2 + \lambda \bullet \left\|s\right\|_1\right\} \tag{5-5}$$

We use the L2 to constrain the residual of observations and reconstructed value and use the L1 norm regularization term to make s sparse.

5.2 Experimental results and analysis

After adding the station number based on the experimental data in chapter 4, about 80 stations for obtaining more GNSS propagation paths,we update the stations' distribution in Figure 5.1.

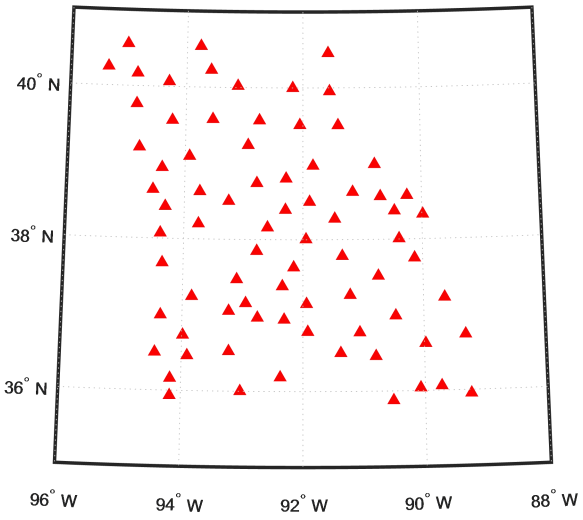

Figure 5.2 American CORS stations distribution on May 10th, 2020

The compressed sensing tomography can reconstruct the ionospheric electronic density based on the GNSS observations and fit the dSTEC and compare them with the input dSTEC.

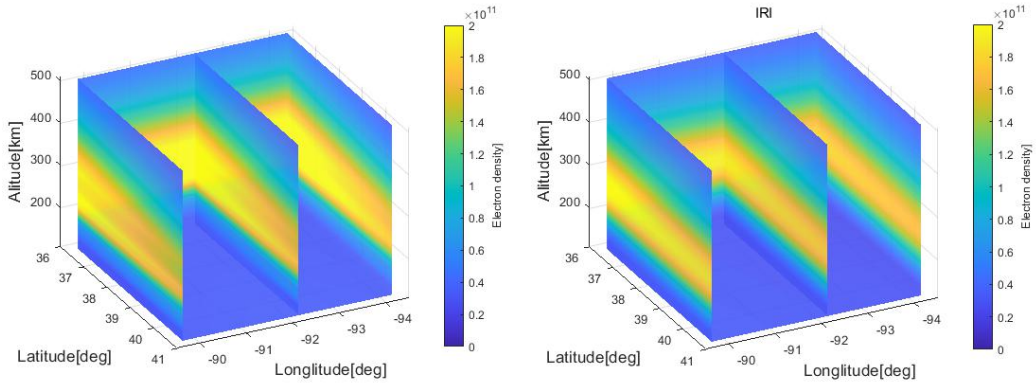

(a) Reconstructed model (b) IRI model

Figure 5.2 reconstructed and IRI electronic density model based on American CORS stations distribution on May 10th, 2020

Figure 5.2(a) is the result of the reconstructed electronic density model, which is similar to the IRI model in Figure 5.2(b). Due to the IRI model has large error comparing to the true electronic density. So we also need to simulate the dSTECs using the reconstructed model and

compare them to the true observations. Figure 5.3 shows the results. The X-axis and Y-axis are the Ray index and dSTEC, respectively. We can see they almost overlap. The root square mean of error between simulated dSTECs and true dSTECs is 0.8 TECU.

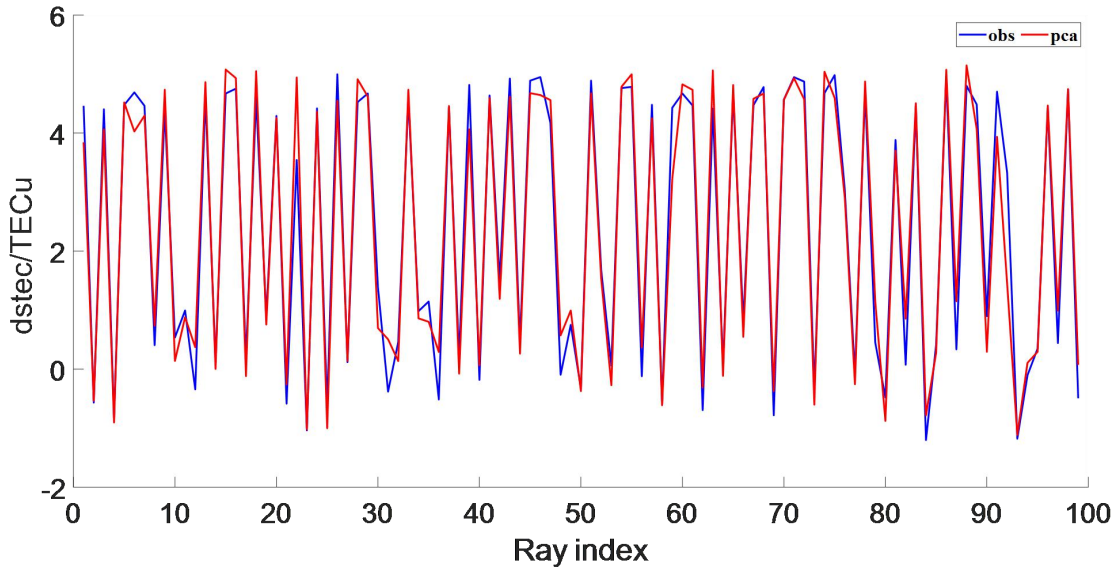

Figure 5.3 Comparison between simulated dSTECs and true dSTECs

5.3 Summary

In this chapter, we introduce the compressed sensing tomographic model to decrease two-dimension ionospheric modeling based on thin shell models' and empirical projection functions' limitations. We use the IRI model as prior information and extract the most significant information using the PCA method. We set the PCA's results as the basis. For input STEC, we use the single difference between satellites to eliminate the receivers' DCB, getting dSTEC. We reconstruct the three-dimension model of the ionospheric layers by compressed sensing methods. Then, we use the three-dimension model to construct the dSTEC and compare it with the input dSTEC. The root means square of error is less than 1TECU

6 Conclusion and Future Work

6.1 Conclusion

This thesis concentrates on the procedure of modeling the ionosphere and illustrates whether the regional high accuracy ionospheric prior model can reduce the convergence time. The piece consists of three aspects: the procedure and error source of precise point positioning, the STEC extracting methods, and ionospheric modeling methods. The following are the major works:

1.the analysis of PPP methods based on the GNSS

This thesis lists three traditional precise point positioning methods and analyzes their features. The stochastic models can weigh observations to make better use of the data. Also, we use the empirical model and free correction data to decrease the effect of the error source in the GNSS propagation. After these processes, we can make the position error under 10 cm. The convergence time will be shortened compared with the traditional IF PPP. It proves the superiority of the method. After the experiments, we can conclude that the UPPP and IF PPP can both get a centimeter-level

2.the STEC extraction methods

This thesis studies the popular STEC extracting methods, illustrating the advantages of the UPPP methods. Through the comparison between the estimated STEC and STEC calculated by GIM, we can see that our estimated results are similar to prior STEC. These data are suitable for modeling later.

3.the ionospheric modeling methods

According to the former work, we gain the estimated STEC. Considering the thin shell model, we put forward the spherical harmonic function model and the polynomial model to model the ionospheric layer. The experimental results represent the regional model can improve the positioning performance.

4.Tomography model

We propose a compressed sensing tomographic model to decrease two-dimension ionospheric modeling based on thin shell models' and empirical projection functions' limitations. We use

experimental data to verify that the model is a high-precision 3D ionospheric electron density model.

6.2 Future Work

Based on the UPPP positioning model, the ionospheric time-delay extraction and regional modeling have been systematically and intensely studied, and we have obtained specific results. However, the study still has some shortcomings:

1. We use four Systems to perform positioning. However, in STEC extraction and modeling, because of the lack of relevant observation data, we mainly study GPS data. We need to investigate further on GLONASS, Galileo, Beidou.

2. When calculating the resolution of UPPP, we use the float resolution. It will make the convergence time longer, which brings a massive noise to the STEC and increase the difficulty of modeling the VTEC ionosphere. The ambiguity resolution fixed methods should be implemented into STEC extraction.

3. The tomography algorithm relies on the prior electronic density models such as IRI or NeQuick. We need to consider some methods to improve the algorithm's robustness.

References

[1]Teunissen, P., Montenbruck O. (ed.). Springer handbook of global navigation satellite systems[M]. Springer, 2017.

[2]Zumberge, J. F. et al., Precise point positioning for the efficient and robust analysis of GPS data from large networks[J]. Journal of Geophysical Research, 1997, 102(3): 5005-5017.

[3]Kouba, J., Heroux, P., Precise Point Positioning Using IGS Orbit and Clock Products[J]. Gps Solutions, 2001, 5(2): 12-28.

[4]Bilitza, D., IRI the International Standard for the Ionosphere[J]. Advances in Radio Science, 2018: 1-11.

[5]Bidaine, B. et al., Nequick: In-depth analysis and new developments[C]. In: 3rd ESA Workshop on Satellite Navigation User Equipment Technologies NAVITEC'2006. 2006. p. 14.

[6]Wilson, B. D.; Mannucci, A. J., Instrumental biases in ionospheric measurement derived from GPS data[C]. 1993.

[7]Kouba, J., Heroux, P., Precise Point Positioning Using IGS Orbit and Clock Products[J]. Gps Solutions, 2001, 5(2): 12-28.

[8]Gao, Y., Shen, X., A New Method for Carrier-Phase-Based Precise Point Positioning[J]. Annual of Navigation, 2002, 49(2): 109-116.

[9]Keshin, M. O. et al., Single and dual-frequency precise point positioning: approaches and performance[C]. In: Proceedings of the 3rd ESA workshop on satellite navigation user equipment technologies, NAVITEC. 2006. p. 11-13.

[10]Collins, P., Isolating and estimating undifferenced GPS integer ambiguities[C]. In: Proceedings of ION NTM-2008, Institute of Navigation, San Diego, California, Jan, pp 720–732, 2008

[11]Ge, M. et al., Resolution of GPS carrier-phase ambiguities in precise point positioning (PPP) with daily observations[J]. J Geod 82(7):389–399, 2008

[12]Laurichesse, D. et al., Zero-difference ambiguity fixing for spaceborne GPS receivers[C]. In: Proceedings of the 21st International Technical Meeting of the Satellite Division of The Institute of Navigation (ION GNSS 2008). 2008. p. 758-768.

[13]Zhang, B. et al., Precision single-point positioning algorithm and application based on GPS dual-frequency original observations[J]. Journal of Surveying and Mapping, 2010, 39(05): 478-483.

[14]Geng, J., Bock, Y., Triple-frequency GPS precise point positioning with rapid ambiguity resolution[J]. Journal of Geodesy, 2013, 87(5): 449-460.

[15]Li, X. et al., Precise positioning with current multi-constellation global navigation satellite systems: GPS, GLONASS, Galileo and BeiDou[R]. Scientific reports, 2015, 5: 8328.

[16]Zhang, B. et al., PPP-RTK based on undifferenced and uncombined observations: theoretical and practical aspects[J]. Journal of Geodesy, 2019, 93(7): 1011-1024.

[17]Bishop, G. J. et al., Multipath effects on the determination of absolute ionospheric time delay from GPS signals[J]. Radio Science, 1985, 20.3: 388-396.

[18]Schaer, S.; SOCIÉTÉ HELVÉTIQUE DES SCIENCES NATURELLES. COMMISSION GÉODÉSIQUE. Mapping and predicting the Earth's ionosphere using the Global Positioning System[J]. Institut für Geodäsie und Photogrammetrie, Eidg. Technische Hochschule Zürich, 1999

[19]Zhang B., et al., Using non-combined precision single-point positioning technology to determine the total electron content of the oblique ionosphere and the deviation of the station satellite differential code[J].Acta Geomatica Sinica,2011,40(04):447-453.

[20]Lanyi, G. E., Roth, T. A comparison of mapped and measured total ionospheric electron content using global positioning system and beacon satellite observations[J]. Radio Science, 1988, 23.4: 483-492.

[21]Mannucci, A. J., et al., A global mapping technique for GPS-derived ionospheric total electron content measurements[J]. Radio science, 1998, 33.3: 565-582.

[22]Fletens, J., et al., Routine Production of Ionosphere TEC Maps at ESOC| First Results[C]. In: Proceedings of the IGS Analysis Center Workshop, edited by JM Dow et al. 1998. p. 273-284.

[23]Hernández-Pajares, M. et al., The IGS VTEC maps: a reliable source of ionospheric information since 1998[J]. Journal of Geodesy, 2009, 83(3-4):263-275.

[24]Gao, Y., Heroux, P., Kouba, J., Estimation of GPS receiver and satellite L1/L2 signal delay biases using data from CACS[C]. In: International Symposium on Kinematic Systems in Geodesy, Geomatics, and Navigation, Univ. of Calgary, Banff, Alberta, Canada. 1994.

[25]Feltens, J., Development of a new three-dimensional mathematical ionosphere model at European Space Agency/European Space Operations center[J]. Space Weather, 2007, 5.12.

[26]Bruno, J. et al., A realistic simulation framework to evaluate ionospheric tomography[J]. Advances in Space Research, 2020, 65(3): 891-901.

[27]Arikan, O. et al., Computerized ionospheric tomography with the IRI model[J]. Advances in Space Research, 2007, 39(5): 859-866.

[28]Wen, D. et al., Three-dimensional ionospheric tomography by an improved algebraic reconstruction technique[J]. Gps Solutions, 2007, 11(4): 251-258.

[29]Wang, K., Kothacher, M., Ambiguity resolution for triple-frequency geometry-free and ionosphere-free combination tested with real data[J]. Journal of geodesy, 2013, 87.6: 539-553.

[30]Montenbruck, O. et al., Differential code bias estimation using multi-GNSS observations and global ionosphere maps[J]. Navigation: Journal of the Institute of Navigation, 2014, 61.3: 191-201.

[31]Barnes, J.B., Ackroyd, N., Cross, P.A., Stochastic modeling for very high Precision real-time kinematic GPS in an engineering environment [C]. In: Proceedings of the F.I.G, XXI International Congress, Commission 6, Engineering Surveys, July 19-25, Brighton, U.K., pp.61-76. (1998).

[32]Hugentobler, U., Schaer, S., Fridez, P., Bernese GPS Software Version 4.2 [R]. Astronomical Institute, University of Bern, February 2001.

[33]King, R.W, Bock, Y., Documentation for the GAMIT GPS Analysis Software [R]. Massachusetts Institute of Technology, Cambridge Mass, (1999).

[34]Liu, X., Quality control and stochastic model refinement of precise GPS dynamic positioning[D]. Wuhan: Wuhan University, 2002

[35]IGS official Web Site, Products, http://www.igs.org/products (October, 2020).

[36]Subirana, J. S., Zornoza, J. M. J., Hern_andez-Pajares, M., GNSS Data Processing, Vol. I: Fundamentals and Algorithms, ESA, Leiden, 2013

[37]Ashby, N., Relativity in the Global Positioning System[J]. Living Reviews in Relativity, 2003, 6(1): 1-42.

[38]Schmid, R. et al., Generation of a consistent absolute phase-center correction model for GPS receiver and satellite antennas[J]. Journal of Geodesy 81(12):781-798. (2007)

[39]Wu, J-T. et al., Effects of antenna orientation on GPS carrier phase[R]. asdy, 1992, 1647-1660.

[40]Petit, G., Luzum, B., IERS conventions (2010). Frankfurt am Main: Verlag des Bundesamts für Kartographie und Geodäsie, Germany.

[41]Montenbruck, O., Hauschild, A., Code biases in multi-GNSS point positioning[C],In: ION ITM 2013, pp, 616-628, 2013.

[42]Niell, A. E., Global mapping functions for the atmosphere delay at radio wavelengths[J], Journal of Geophysical Research, 101 (B2), 3227-3246, 1996.

[43]Boehm, J., Niell, A., Tregoning, P., Schuh, H., Global Mapping Function (GMF): A new empirical mapping function based on numerical weather model data[R], Geophysical Research Letters, 33, L07304, 2006.

[44]Boehm, J.,Werl, B., Schuh, H., Troposphere mapping functions for GPS and very long baseline interferometry from European center for Medium-Range Weather Forecasts operational analysis data[J], Journal of Geophysical Research, 111, B02406, 2006.

[45]Klobuchar, J. A., Ionospheric time-delay algorithm for single-frequency GPS users[J]. IEEE Transactions on aerospace and electronic systems, 1987, 3: 325-331.

[46]Yang, C. et al., Assessment and Comparison of Broadcast Ionospheric Models: NTCM-BC, BDGIM, and Klobuchar[J]. Remote Sensing, 2020, 12.7: 1215.

[47]Xiang, Y., Carrier phase-based ionospheric modeling and augmentation in uncombined precise point positioning (UPPP). 2018.

[48]Liu, Z., A new automated cycle slip detection and repair method for a single dual-frequency GPS receiver[J], Journal of Geodesy, 85, 171-183, 2011.

[49]Deo, M., El-Mowafy, A., Cycle Slip and Clock Jump Repair with Multi-Frequency Multi-Constellation GNSS data for Precise Point Positioning[C], International Global Navigation Satellite Systems Society Symposium, 14-16 July, Outrigger Gold Coast, Qld Australia, 2015.

[50]Guo, F., Theory and Methodology of Quality Control and Quality Analysis for GPS Precise Point Positioning[C]. Wuhan University Press, 2016

[51]Böhm, J., Schuh, H. (ed.), Atmospheric effects in space geodesy[J]. Berlin: Springer, 2013.

[52]Buonsanto, M. J., Ionospheric storms—A review[J]. Space Science Reviews, 1999, 88.3-4: 563-601.

[53]Komjathy, A., Global ionospheric total electron content mapping using the Global Positioning System[M]. University of New Brunswick, (1997)

[54]Bai, M. et al., Experimental study on the motion of corona ionospheric ions under atmospheric pressure[J]. Nuclear Fusion and Plasma Physics, 2005, 025(004):311-314.

[55]Misra, P., Enge, P., Global Positioning System: signals, measurements and performance second edition. Global Positioning System: Signals[C], Measurements And Performance Second Editions, 2006, 206.

[56]Petrie, E. J. et al., A review of higher order ionospheric refraction effects on dual frequency GPS[R]. Surveys in geophysics, 2011, 32.3: 197-253.

[57]Gao, Y., GNSS biases, their effect and calibration[C]. In: IGS Workshop. 2008.

[58]Schaer, S., and Société helvétique des sciences naturelles. Commission géodésique. Mapping and predicting the Earth's ionosphere using the Global Positioning System[C]. Vol. 59. Institut für Geodäsie und Photogrammetrie, Eidg. Technische Hochschule Zürich, 1999.

[59]Georgiadiou, Y., Modeling the ionosphere for an active control network of GPS stations[M]. LGR-series-publications of the Delft Geodetic Computing center, 1994.

[60]Hernandezpajares M. et al., The ionosphere: effects, GPS modeling and the benefits for space geodetic techniques[J]. Journal of Geodesy, 2011, 85(12): 887-907.

[61]Dunteman, G. H., Principal components analysis[R]. Sage, 1989.

[62]Eldar, Y. C.; Kutyniok, G. (ed.)., Compressed sensing: theory and applications[M]. Cambridge university press, 2012.

[63]Donoho, D. L., Compressed sensing[J]. IEEE Transactions on information theory, 2006, 52.4: 1289-1306.

[64]Sui, Y. et al., Sparse Reconstruction of Regional Ionospheric Tomography Based on Beidou Ground Based Augmentation System[C]. In: China Satellite Navigation Conference. Springer, Singapore, 2020. p. 673-683.

[65]Deng Y., Ridley A. J., The Global Ionosphere-Thermosphere Model and the Nonhydrostatic Processes[M], Modeling the Ionosphere–Thermosphere System. American Geophysical Union (AGU), 2014.

[66]Kolb P.F., Chen, X., Vollath, U., A New Method to Model the Ionosphere Across Local Area Networks[J]. Proceedings of International Technical Meeting of the Satellite Division of the Institute O, 2005.

[67]Xue J.C., Song S.L. , Zhu W. Y., Global ionosphere model based on BDS/GPS dual-system observations[J]. entia Sinica, 2015, 45(7):079505.

Acknowledgement

Time flies, thinking back to the past, I spent a meaningful graduate career. Here, I want to thank my supervisors, Ph.D Tuan Nguyen and Professor Haiyang Fu, for their patient guidance and significant suggestions. I have learned a lot in life and study with their help. It is my most tremendous honor to learn from them.

I would also like to thank all professors in the Key Laboratory of EMW information for their help in my research. Thank FDU and UTU for providing an excellent environment, which let me learn much knowledge and develop good habits.

Furthermore, thanks to all my classmates, i.e. senior sister Yun Sui, junior brother Kangning Wang, Zenghui Shi for their help. Thanks for helping me solve my problems patiently.

Finally, I also need to thank my family for helping me with financial and spiritual support. Thanks to my wife, Mengli Cui, for care for my life and academic support, which help me to overcome every difficulty in my life.